Physics of the Earth and Planetary Interiors 308 (2020) 106552

Contents lists available at ScienceDirect

Physics of the Earth and Planetary Interiors

journal homepage: www.elsevier.com/locate/pepi

Discriminating lower mantle composition

C. Houser[a,*], J.W. Hernlund[a], J. Valencia-Cardona[b], R.M. Wentzcovitch[a,c,d]

[a] Earth-Life Science Institute, Tokyo Institute of Technology, Meguro-ku, Tokyo, Japan
[b] Scientific Computing Program, University of Minnesota, Twin Cities, Minneapolis, MN, USA
[c] Department of Applied Physics and Applied Mathematics, Columbia University, New York, NY, USA
[d] Department of Earth and Environmental Sciences, Lamont-Doherty Earth Observatory, Columbia University, Palisades, NY, USA

ARTICLE INFO

Keywords:
Lower mantle
Global seismology
Mantle composition
Mantle temperature

ABSTRACT

Constraining Earth's bulk composition is fundamental to understanding our planet's formation and evolution. While the lower mantle accounts for a majority of the bulk silicate Earth, it is also the least accessible. As experimental and theoretical mineral physics constraints on mineral elasticity at lower mantle temperatures and pressures have improved, comparisons between predicted seismic velocity and density profiles for hypothesized bulk compositions and 1D seismic models have become commonplace. However, the degree to which a given composition is a better or worse fit than another composition is not always reported, nor are the influences of the assumed temperature profile and other uncertainties discussed. Here we compare seismic velocities and densities for perovskitite, pyrolite, and harzburgite bulk compositions calculated using advanced *ab initio* techniques to explore the extent to which the associated uncertainties affect our ability to distinguish between candidate compositions. We find that predicted differences between model compositions are often smaller than the influence of temperature uncertainties and therefore these comparisons lack discriminatory power. The inability to distinguish between compositions is largely due to the high sensitivity of seismic properties to temperature accompanied by uncertainties in the mantle geotherm, coupled with diminished sensitivity of seismic velocity to composition toward the base of the mantle. An important exception is the spin transition in (Mg,Fe)O-ferropericlase, which is predicted to give a distinct variation in compressional wave velocity that should distinguish between relatively ferro-magnesian and silica-rich compositions. However, the absence of an apparent spin transition signature in global 1D seismic profiles is a significant unresolved issue in geophysics, and it has important geochemical implications. The approach we present here for establishing discriminatory power for such comparisons can be applied to any estimate of seismic velocities and associated uncertainties, and offers a straightforward tool to evaluate the robustness of model comparisons.

1. Introduction

The Earth's lower mantle (~660–2890 km depth) occupies 55% of our planet's volume and constitutes 72% of the rocky silicate mass. Its properties determine the exchange of heat and mass between the surface and the core and thus many aspects of planetary evolution. Owing to its great depth, direct sampling is beyond the horizon and few processes are capable of bringing unaltered samples to the surface. Recently, diamond inclusions have contributed valuable information regarding mantle composition variability (Pearson et al., 2014; Tschauner et al., 2018; Nestola et al., 2018) but these are unlikely to be representative samples of typical mantle. Since we must rely on inference from remote sensing methods such as seismic tomography and gravity, the bulk chemical composition, the average thermal gradient, and their regional variations remain poorly constrained.

If the lower mantle composition is similar to that inferred for the upper mantle (i.e., peridotite-like), then it is expected to be dominated by (Mg,Fe)SiO_3-bridgmanite (~80%) along with (Mg,Fe)O-ferropericlase (~20%) and a minor amount of $CaSiO_3$-perovskite. However, owing to the long history of subduction/recycling of oceanic lithosphere into the mantle (Cawood et al., 2006), the isotopic and compositional diversity of volcanic lavas (Hofmann, 1997), seismic tomography models where vertical fast and slow material suggests the exchange of material across the mantle (Houser and Williams, 2009), and large seismically distinct regions in the lowermost mantle (Hernlund and Houser, 2008; Deschamps et al., 2012; Cottaar and Lekic, 2016; Garnero et al., 2016), one may infer that the Earth's lower mantle is host to variable rock types at a variety of length scales.

* Corresponding author.
E-mail address: chouser@elsi.jp (C. Houser).

https://doi.org/10.1016/j.pepi.2020.106552
Received 23 June 2018; Received in revised form 28 April 2020; Accepted 10 July 2020
Available online 23 July 2020
0031-9201/

Isotopic evidence for long-lived lower mantle heterogeneity also continues to unfold, such as anomalies in ^{182}W or ^{129}Xe measured in ocean island basalt (OIB) lavas that must have been generated during Earth's formation and persisted over billions of years of mantle evolution (Mukhopadhyay, 2012; Mundl et al., 2017).

In spite of its *a priori* expected isotopic and chemical heterogeneity, there have been numerous attempts to constrain a single characteristic composition for the lower mantle by comparison of mineral physics and seismic data. Such comparisons are becoming more commonplace owing to the increasing availability of numerical tools for predicting geophysical properties of the mantle based on candidate compositions, for example PERPLEX (Connolly, 2009), HeFESTo (Stixrude and Lithgow-Bertelloni, 2011), and BurnMan (Cottaar et al., 2014). The typical approach is to compute velocities and densities derived from equation of state and elasticity constraints using laboratory experiments and/or *ab initio* calculations for hypothesized compositions and compare the results to average radial 1D profiles of seismic velocity and density such as PREM (Dziewonski and Anderson, 1981) or ak135 (Kennett et al., 1995). This procedure (e.g., da Silva et al., 2000; Karki et al., 2001; Wentzcovitch et al., 2004; Stixrude and Lithgow-Bertelloni, 2005; Mattern et al., 2005; Cammarano et al., 2005; Matas et al., 2007; Khan et al., 2008; Cobden et al., 2009; Wang et al., 2015; Wolf et al., 2015; Wu, 2016) requires a specified geotherm and bulk composition which are used to compute the identity and abundance of individual mineral phases using a thermodynamic equilibrium model. The results are then coupled with estimates of the thermoelastic properties and equations of state of the constituent phases, and finally one applies a suitable averaging scheme to obtain the seismic properties of an aggregate model rock in terms of compressional, shear, and bulk sound velocity (V_P, V_S, V_C, respectively) as well as density (ρ). These predictions are then evaluated for their agreement with 1D seismic models.

What has often been lacking in such approaches is a quantitative means to demonstrate the goodness of fit between different composition models, or a straightforward way to consider the influence of uncertainties. The comparison of predictions to the 1D seismic models is only useful if the compositions being compared exhibit readily distinguishable seismic properties. Also, the seismic observations that are chosen for comparison must be sensitive to the potential range of composition variations, and be sufficiently accurate to resolve the differences. Furthermore, differences in quantitative predictions between candidate compositions should be larger than the uncertainties involved, otherwise the comparisons "fall within the error bars." It is also important to identify unconstrained degrees of freedom in the comparisons in order to establish the uniqueness of the results, and the occurrence of trade-offs with other correlated factors.

Progress in quantifying the influence of uncertainties on model outcomes has been made using error propagation in mapping input mineral physics parameters to predictions for the temperature, composition, and state of the lower mantle (Trampert et al., 2001; Trampert et al., 2004; Resovsky et al., 2005; Deschamps and Tackley, 2008, 2009; Cobden et al., 2009; Mosca et al., 2012; Connolly and Khan, 2016). Such studies reveal the extent to which uncertainties in the some of the important input parameters lead to variability in predicted outcomes. Trampert et al. (2004) and Deschamps and Tackley (2008) focused on the propagation of errors through the inversion of seismic data for 3D temperature and composition anomalies. Cobden et al. (2009) explored the predicted seismic velocities for a variety of compositions and thermal profiles for different equation of state methods and compared the results to shear and compressional velocity ratios and gradients at different depth ranges for the lower mantle. This latter study propagated estimated uncertainties in the elastic parameters into uncertainty contours in predicted seismic properties, and acknowledged that only differences observed outside these contours should be considered valid for differentiating candidate scenarios. These studies motivate a broader discussion and generalization of these ideas to include all potential uncertainties that might arise in this kind of exercise.

Here we aim to determine the basic conditions for which it is possible to distinguish between lower mantle composition scenarios in light of uncertainties when comparing predictions to seismic constraints. We also propose a means to evaluate the fundamental question: At a given depth, is it possible to know the temperature well enough to discern the composition? We develop a basic tool to quantitatively measure the degree of "discriminatory power" in comparing various competing scenarios. We apply this strategy to perovskitite, pyrolite, and harzburgite compositions using our latest *ab initio* techniques. We then examine whether the degree of uncertainty required to distinguish between these candidate scenarios can be satisfied given our current knowledge of mantle temperature. Our findings demonstrate that the magnitude of the temperature uncertainty alone often exceeds predicted differences in candidate compositions, and therefore such 1D comparisons do not sufficiently favor any particular lower mantle composition at the present time. Alternative approaches are therefore needed to pursue the use of seismological constraints to make inferences regarding mantle composition. However, the largest discriminatory power is found in the compressional wave velocity in the mid-lower mantle, owing to the predicted effects of a spin transition in ferropericlase. A global signal due to this spin transition should be present if the lower mantle is pyrolitic, but is not observed. We discuss the implications of this finding, and suggest possible strategies to resolve this inconsistency.

2. Methods

In this section we outline our methods to evaluate the robustness of comparing predicted physical properties to 1D seismic profiles. First, we describe our methods for obtaining example seismic properties for different compositions using *ab initio* calculations. Next, we outline a simple tool for comparing candidate composition scenarios that accounts for the fact that differences must exceed an error/uncertainty threshold in order to have "discriminatory power." In later sections, we discuss the types of error that contribute to our calculations and suggest strategies for applying the discriminatory power metric.

2.1. Calculating seismic velocity and density

We focus on three compositions which demonstrate how seismic velocity and density respond to changes in the abundance of ferropericlase in the lower mantle. Pyrolite is a model rock composition constructed by remixing of oceanic crust and its underlying mantle lithosphere (Ringwood, 1962). It represents rock that has either never been melted at mid-ocean ridges or has been thoroughly remixed and homogenized to the grain scale. If the lower mantle were indeed pyrolite then the Earth's whole mantle Mg/Si ratio would be similar to that of the upper mantle (~1.2), a value higher than that of the Sun's photosphere (close to 1). While silicon may reside as an alloy in the core (Allegre et al., 1995; Rubie and Jacobson, 2016), its storage capacity may be limited to values lower than needed in order for the Earth to match solar values (Badro et al., 2015; Ozawa et al., 2016). If the lower mantle were more Si-rich than the upper mantle, then it would be almost entirely perovskite (bridgmanite) and calcium perovskite, which we call perovskitite for this exercise. We also include harzburgite because it is the main constituent of subducting oceanic lithosphere. Seismic tomography reveals that subducted lithosphere enters the lower mantle beneath subduction zones. While some subducted slabs may "stagnate" (Fukao et al., 2009; Fukao and Obayashi, 2013) many major ancient subduction centers reveal slabs penetrating through the lower mantle to the core mantle boundary region (Houser et al., 2008). The main difference in our compositions is the relative proportion of the (Mg,Fe)O-ferropericlase phase, with the perovskitite model containing no ferropericlase and harzburgite being enriched in ferropericlase relative to pyrolite. With these three compositions we cover a range of Mg/Si that spans most of the meteorites sampled in our solar system

(Palme and O'Neill, 2014).

In the comparisons that follow, we use *ab initio* calculations to predict seismic velocities and density. Our calculations are based on previously published results on ferropericlase and bridgmanite (Wentzcovitch et al., 2009; Wu et al., 2009; Wu et al., 2013; Shukla et al., 2015). These calculations used the local density approximation (LDA) (Ceperley and Alder, 1980) and LDA plus Hubbard U (LDA + U) methods (Cococcioni and de Gironcoli, 2005; Kulik et al., 2006; Hsu et al., 2009). All of these calculations included the same pseudopotentials. The pseudopotentials for Fe, Si, and O were generated using Vanderbilt's method (Vanderbilt, 1990). For ferropericlase the non-self consistent Hubbard U (Cococcioni and de Gironcoli, 2005) was applied, but for Fe-bearing bridgmanite we used self-consistent (Kulik et al., 2006) and structurally consistent U (Hsu et al., 2009) as reported by Hsu and Wentzcovitch (2014).

Thermodynamic properties of ferropericlase and bridgmanite were obtained using the quasiharmonic approximation (QHA) (Carrier et al., 2007). For ferropericlase the phonon spectrum was obtained using a vibrational virtual crystal (Wentzcovitch et al., 2009; Wu et al., 2009) developed after phonon dispersions of MgO obtained using density functional perturbation theory (DFPT) (Baroni et al., 2001), while for bridgmanite all phonon dispersions in the iron bearing systems were obtained using DFPT + U (Floris et al., 2011). For the Mg end-members MgO and $MgSiO_3$, the QHA is an effective approximation as previously indicated (Wentzcovitch et al., 2010). This approximation is also well-suited for ferropericlase as there are no softening of phonon mode frequencies in any spin state for the entire pressure range of the mantle (Marcondes et al., 2019). The thermodynamic and thermoelastic properties of $CaSiO_3$ were reproduced (Kawai and Tsuchiya, 2014, 2015) using a Mie-Debye-Grüneisen formalism and were published in Supplementary material in (Valencia-Cardona et al., 2017). The properties of individual minerals were calculated using an ideal solid solution formalism, where the end-members were the Mg-compound and a (Mg,Fe) solid solution with Mg = 0.875 and Fe = 0.125 for bridgmanite (Shukla et al., 2015) and Mg = 0.8125 and Fe = 0.1875 for ferropericlase (Wu et al., 2013). For intermediate compositions the thermoelastic properties were linearly interpolated. This procedure shows good agreement with experiments for both minerals (Wu et al., 2013; Shukla et al., 2015).

The compositions we investigate here are considered mixtures of SiO_2 - MgO - CaO - FeO - Al_2O_3. Although the Fe—Mg partitioning coefficient between bridgmanite and ferropericlase is expected to vary throughout the lower mantle because of the spin crossover (Irifune et al., 2010; Piet et al., 2016), we have examined aggregates with uniform iron partitioning equal to 0.5, which is consistent with those reported by Irifune et al. (2010). Table 1 shows weight and mole percentages of oxides in the aggregates considered. Aggregate elastic properties were obtained using the Voigt-Reuss-Hill average for three candidate compositions: perovskitite consisting of 94 wt% bridgmanite and 6 wt% calcium perovskite; pyrolite consisting of 76 wt% bridgmanite, 17 wt% ferropericlase, and 7 wt% calcium perovskite; and harzburgite consisting of 74 wt% bridgmanite, 24 wt% ferropericlase, and 2 wt% calcium perovskitite. The bridgmanite phase hosts 8% Fe and 5% Al $(Mg_{0.87},Fe_{0.08},Al_{0.05})SiO_3$ while the ferropericlase hosts 15% Fe $(Mg_{0.85},Fe_{0.15})O$.

The results for V_P, V_C, V_S, and ρ are shown in Fig. 1 for the perovskitite, pyrolite, and harzburgite compositions described in Table 1. PREM values are represented as black circles whose size approximates our assumed uncertainties since the errors are not explicitly stated (see Supplementary material). The dip in V_P and V_C in the mid mantle pyrolite and harzburgite compositions is due to the high-spin to low-spin transition in iron which decreases the bulk modulus of ferropericlase (Wentzcovitch et al., 2009; Marquardt et al., 2018). The high-to-low spin transition in iron in bridgmanite has been found when Fe^{3+} occupies the B site of the perovskite structure (Catalli et al., 2010; Hsu et al., 2011; Lin et al., 2012; Mao et al., 2015; Fu et al., 2018). However, most of the Fe^{3+} and all the Fe^{2+} occupy the A site in the presence of Al and remain in the high spin state throughout the lower mantle (Lin et al., 2016; Hsu et al., 2012). As such, there is no seismic expression of the spin transition in bridgmanite when Al is present (Shukla et al., 2016), although a softening of the bulk modulus in Al-free bridgmanite has been reported (Fu et al., 2018). Since we have included Al, all the iron is Fe^{2+} in the A site in bridgmanite (Valencia-Cardona et al., 2017). The variation in seismic velocities and densities predicted for these composition models varies continuously from perovskitite to harzburgite, with pyrolite exhibiting intermediate values. The differences are most apparent comparing harzburgite relative to perovskitite due to the distinct properties of ferropericlase that is abundant in the former but absent in the latter.

We include an equation of state (EoS) extrapolation to demonstrate the variability in the mineral physics predictions which arise from different methods. Cottaar et al. (2014) provide the BurnMan tool which can compute the outcomes of using different EoS approaches and input parameters. We modified their code which computed pyrolite velocities and density in their Fig. 7. They used an anchor temperature of 2000 K at 32 GPa as it provided the best fit to PREM for their parameterization (the light green line in Fig. 4). We lowered the anchor temperature to 1935 K using their model in order to match the temperature in our calculations. Since they also made different assumptions regarding how the iron is distributed between bridgmanite and ferropericlase, we adjusted the code to match the 0.5 value for partioning used in our *ab initio* calculations. These modifications produce the EoS results for pyrolite, shown as the dashed green line in Fig. 1. In addition, they did not include calcium perovskite while our implementation has lower velocity for calcium perovskite (CaPv) than for bridgmanite. The CaPv behavior is still debated (Caracas et al., 2005; Kawai and Tsuchiya, 2015; Valencia-Cardona et al., 2017), and the influence of assumptions regarding partitioning and the contribution of minor phases should be considered as a source of error. With the exception of the inflection due the spin transition (which is not accounted for in the EoS prediction), our *ab initio* pyrolite (blue) and the EoS pyrolite (dashed green) are difficult to distinguish in *Vs* and density.

As in other studies, the geotherms used to produce the curves in Fig. 1 use “self-consistent” isentropic gradients obtained from the *ab initio* calculations. The temperature at the top of the lower mantle is anchored at 1873 K, compatible with the post-spinel phase transition at 660 km depth (Irifune et al., 1998). We do not extend these calculations to the core-mantle boundary (~136 GPa) since this study does not address the numerous potential complexities associated with the core-mantle boundary region (Hernlund and McNamara, 2015). Our

Table 1
Compositions used in this study in wt% (mole %). We calculate the velocities, density, and self consistent thermal profile (isentrope) for pyrolite (McDonough and Sun, 1995), harzburgite (Baker and Beckett, 1999) and perovskitite (Williams and Knittle, 2005). The main difference in these compositions is the amount of ferropericlase (Fp): harzburgite 24 wt% Fp, pyrolite 17 wt% Fp, perovskitite 0 wt% Fp.

	SiO_2	MgO	FeO	CaO	Al_2O_3
Perovskitite	52.83 (48.91)	31.18 (40.06)	7.58 (5.86)	3.0 (2.97)	4.0 (2.18)
Pyrolite	45.00 (39.37)	37.80 (49.30)	8.05 (5.89)	3.55 (3.33)	4.09 (2.11)
Harzburgite	43.51 (36.07)	45.73 (56.51)	8.76 (6.07)	0.91 (0.81)	1.09 (0.53)

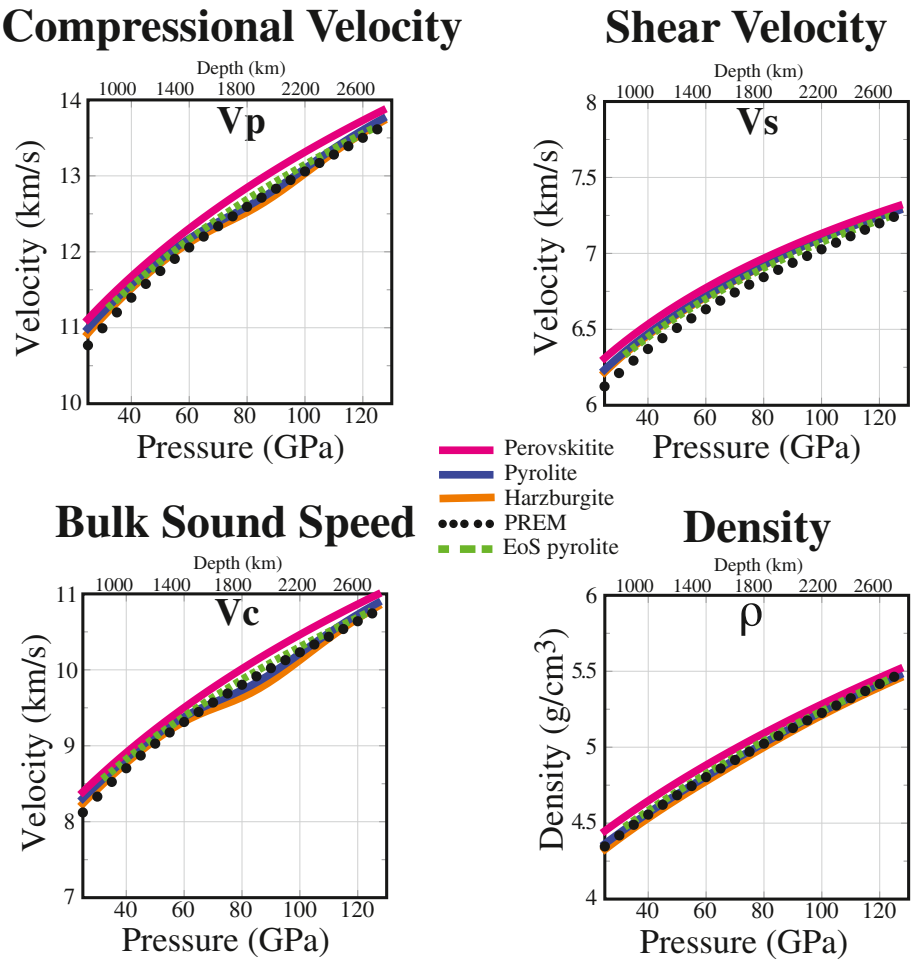

Fig. 1. Calculated velocities and density using the *ab initio* methods described in Section 2.1 for perovskitite (magenta), pyrolite (blue), harzburgite (orange) as well as an EoS calculation for pyrolite (dashed green) using a modified BurnMan (Cottaar et al., 2014) approach (see Section 2.1 text for details) and PREM (black dots) for compressional velocity (V_P, top left), shear velocity (V_S, top right), bulk sound speed (V_C, bottom left) and density (ρ, bottom right). The velocities/density and PREM are plotted with similar width. (For interpretation of the references to colour in this figure legend, the reader is referred to the web version of this article.)

calculations avoid the phase transition of bridgmanite to post-perovskite which occurs near the base of the mantle (Murakami et al., 2004; Oganov and Ono, 2004), and the large low shear velocity provinces which appear to have a composition that is distinct from the rest of the mantle (e.g., Trampert et al., 2004; Hernlund and Houser, 2008).

The convergence of seismic velocities and density in the lower mantle is apparent when plotting their predicted variation in response to changes in temperature and composition (Fig. 2). For a given composition, harzburgite, pyrolite, and perovskitite, we show the change in seismic velocity and density for the material at hot and cold temperatures compared to ambient temperature (i.e., the self-consistent geotherm results in Fig. 1). To obtain the predictions for the hot and cold cases we increased/decreased the anchor temperature at the top of the lower mantle by ± 500 K for the *ab initio* calculations described above. The undulating curves for harzburgite and pyrolite in compressional velocity and bulk sound speed in the mid-mantle are due to the temperature-dependence of the iron spin transition in ferropericlase (Wu and Wentzcovitch, 2014). The grey lines are the difference between the predicted velocities and densities for ambient perovskitite versus ambient harzburgite, while the black lines are for ambient perovskitite versus ambient pyrolite. Compressional velocity and bulk sound speed are most sensitive to composition in the mid-mantle owing to the spin transition in ferropericlase while shear velocity and density are most sensitive to composition at the top of the lower mantle.

2.2. Discriminatory power of model comparisons

Our next task is to establish a robust comparison between mineral physics predictions and geophysical constraints. Consider a particular property Y (such as V_P, V_C, V_S, or ρ) at a position $\vec{r}$ in the Earth, for which we desire to compare a predicted mineral physics value Y_{pred} with geophysically constrained model value Y_{mod}. We can write the geophysical constraint as,

$$Y_{mod}(\vec{r}) = Y_{earth}(\vec{r}) + \varepsilon_{mod}(\vec{r}) \quad (1)$$

where Y_{mod} is the geophysical model value and ε_{mod} is the cumulative error of the model in comparison to the exact value Y_{earth} (i.e., the value in the Earth itself). Errors of this kind will always exist because the observations are presented to us as models (e.g., parameterized fits) derived from data, rather than as raw data which also contains intrinsic measurement errors. Y_{earth}, Y_{mod} and ε_{mod} vary with position $\vec{r}$ inside the Earth. These might also depend upon time t, if the property varies on the time scale of observations, but for the purposes of the present study we will consider the situation to be static.

For the mineral physics prediction of property Y we similarly define,

$$Y_{pred}(P, T, X) = Y_{real}(P, T, X) + \varepsilon_{pred}(P, T, X) \quad (2)$$

where Y_{pred} is the prediction (based on combining experimental data and simulations) and ε_{pred} is the cumulative error in generating the particular mineral physics prediction. In this case Y_{real} is the exact value

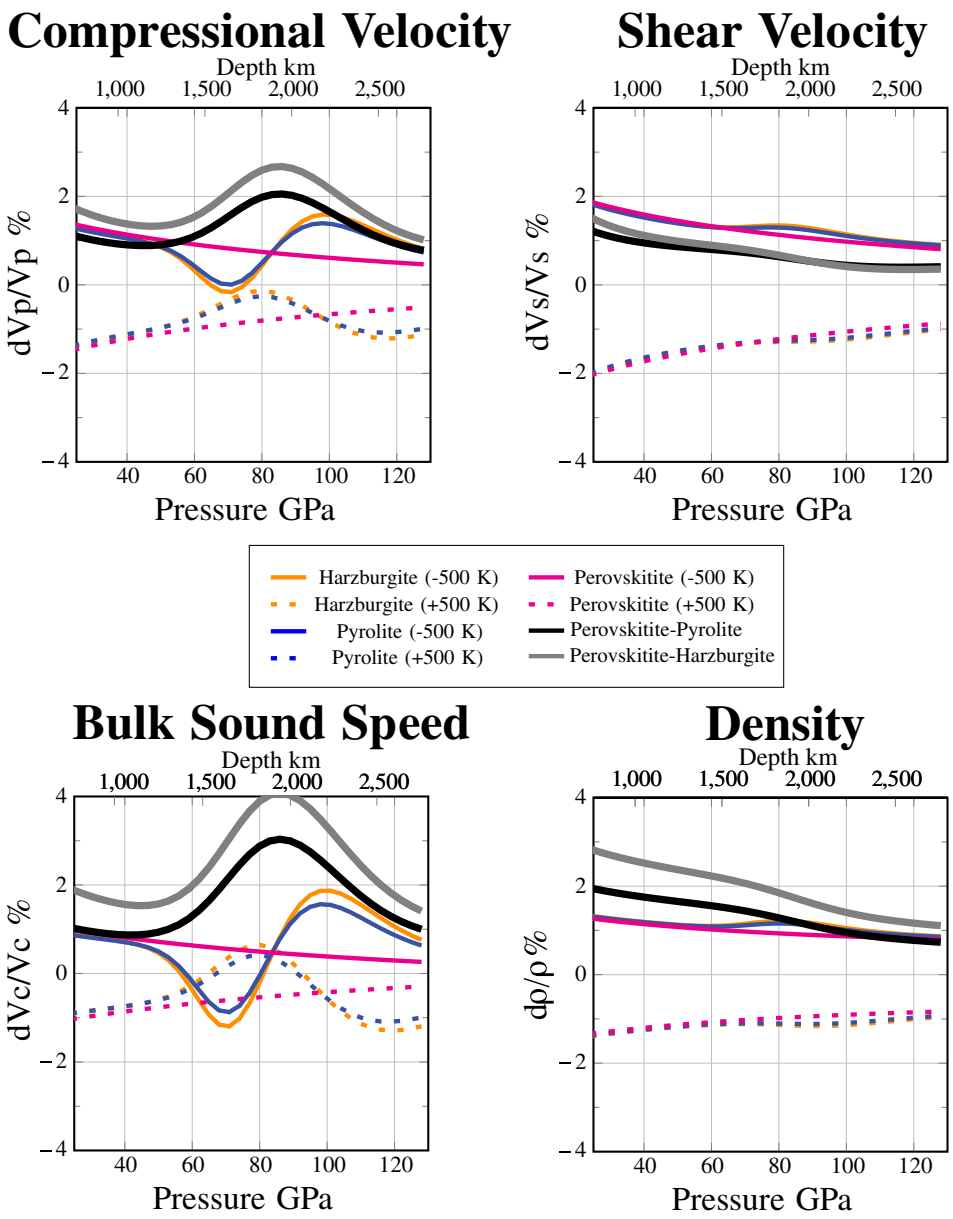

Fig. 2. Predicted velocity and density anomalies for changes in temperature for a uniform composition of harzburgite (orange), pyrolite (blue), and perovskitite (magenta). The *ab initio* calculations were carried out for each composition with a 500 K temperature decrease and a 500 K temperature increase at the top of the lower mantle compared to the ambient values which have an anchor temperature of 1873 K. The high-to-low spin crossover in ferropericlase is temperature dependent, so the anomalies for temperature increase (dashed lines) are not simply a mirror image of those for a temperature decrease (solid lines). The grey line is the difference between the predicted velocities and densities for ambient perovskitite versus ambient harzburgite while the black line is for ambient perovskitite versus ambient pyrolite. Note that changing the temperature by only 500 K produces the same magnitude of a velocity or density anomaly as the entire range of compositions explored here. (For interpretation of the references to colour in this figure legend, the reader is referred to the web version of this article.)

that a hypothesized rock at a specified P, T, X (pressure, temperature, and bulk composition, respectively) would exhibit under assumed conditions. Here the composition X is a placeholder that represents a list of the proportions of each chemical component in the mixture comprising a rock. While Y_{pred}, Y_{real}, and ε_{pred} depend on P, T, X, these can also be defined as a function of $\vec{r}$ if the spatial variation in these parameters is known (i.e., $P = P(\vec{r})$, $T = T(\vec{r})$, and $X = X(\vec{r})$).

Comparison of candidate models to data is usually approached by defining a "misfit" metric, such as an integral of cumulative differences over a volume V,

$$M = \int_V |Y_{pred} - Y_{mod}| dV \tag{3}$$

where the goal is to find the scenario that gives the minimum value of M. Computing M from Eqs. (1)–(3) we see that:

$$M = M_{ideal} + M_{err}, \tag{4}$$

where,

$$M_{ideal} = \int_V |Y_{real} - Y_{earth}| dV, \tag{5}$$

and

$$M_{err} = \int_V |\varepsilon_{pred}| + |\varepsilon_{mod}| dV. \tag{6}$$

M_{err} is the contribution of model uncertainties to the misfit, and arises from errors in both mineral physics predictions as well as errors coupled to the geophysical observations. Note that the way M_{err} is written in Eq. (6), all sources of error are considered to be cumulative.

A key issue is raised by the existence of errors in the comparisons, arising from methodological errors or other sources of uncertainty. While we desire to measure M_{ideal}, in reality we are only practically able to measure M, which contains contributions from both M_{ideal} and M_{err}. Therefore, we must account for an intrinsic error floor that is represented by M_{err}. *In other words, M_{err} establishes the effective resolving power of the comparison between predictions and geophysical models.*

The error floor is relevant for comparing different candidate predictions. Consider an example situation with 2 composition candidates, X_1 and X_2. After computing the corresponding misfits M_1 and M_2, the misfit for model X_1 is found to be much smaller than that for X_2 (i.e., $M_1 \ll M_2$). However, this is not sufficient to demonstrate that model X_1 is a better candidate composition than model X_2 without comparing

their difference relative to the expected error floor M_{err}. If the models do not exhibit differences greater than M_{err}, then their relative comparison is not meaningful (the differences "fall within the error bars"). Note that this holds true regardless of the relative magnitudes of M_1 and M_2.

In order to demonstrate the robustness of a 1D model comparison, it will be useful to define a metric that measures "discriminatory power." A simple measure of discriminatory power for one scenario i relative to another scenario j can be defined as:

$$D_{ij} = \left| \frac{M_i - M_j}{M_{err,ij}} \right|, \tag{7}$$

where,

$$M_{err,ij} = \mathrm{avg}(M_{err,i}, M_{err,j}), \tag{8}$$

and $M_{err,i}$ is given by (6) for model i. Here we employ an average of the two model misfits. In practice, one should choose the kind of averaging scheme that best suits the particular case at hand. For instance if $M_{err,i} \gg M_{err,j}$ then the arithmetic average may not be appropriate. Also, the uncertainty can be depth dependent so simple averaging may not be suitable at all depths depending on Y_{mod} and Y_{pred}.

The preceding discussion, combined with the definition given by Eq. (7), suggests that a comparison between scenarios i and j is only meaningful if $D_{ij} > 1$. How much greater than unity should D_{ij} become in order to establish confidence in the comparison? This is a matter of subjective judgment, however, it is clear that $D_{ij} \approx 1$ is marginal, particularly if the errors are not easy to estimate or can only be stated as lower bounds. In any case, for the purposes of demonstrating discriminatory power, the threshold value of D_{ij} should be justified when making a comparison, and higher values will build more confidence in the ability to distinguish between competing scenarios.

Note that the discriminatory power as defined above applies to a property Y by itself, and addresses the question of whether differences in candidate scenarios can in principle be compared to one another in light of uncertainties using that particular property alone. One may ask whether any gain can be found by linearly combining multiple properties together and seeking the best fit for their combination in this context. Consider 2 properties Y' and Y'' with misfits M' and M'' respectively, and having individual discriminatory powers of D_{ij}' and D_{ij}''. Suppose that we seek to minimize the combined misfit $M' + M''$ for both properties simultaneously, in which case we arrive at a combined discriminatory power,

$$D_{comb,ij} = \left| \frac{M_i' + M_i'' - M_j' - M_j''}{M_{err,ij}' + M_{err,ij}''} \right| = \theta D_{ij}' + (1-\theta) D_{ij}'' < \max(D_{ij}' D_{ij}''), \tag{9}$$

where $\theta = M_{err,\,ij}'/(M_{err,\,ij}' + M_{err,\,ij}'')$ and the last inequality follows because $0 < \theta < 1$. From this result it is clear that there is no gain to be found by the linear combination of the 2 properties Y' and Y'' in terms of increasing the raw discriminatory power. While it is desirable to match multiple observations in practice, each measure is best left to stand alone when applying this metric.

3. Types of uncertainties and application to discriminatory power

3.1. Examples of error/uncertainty

Here we briefly discuss some of the kinds of errors that may confound comparisons between predictions and geophysical models. The definitions for types of uncertainty that follow are not unique, nor are they intended to be comprehensive. However, the language and methods established here will be useful in clarifying our later discussions.

3.1.1. Methodological error

Methodological error arises due to any deficiencies in the methods (and related assumptions) that are employed to compute predicted quantities Y_{pred}. Methodological errors include inaccuracies in the tools/methods themselves, such as those associated with experimental measurements or computational approximations needed to generate the predicted properties. Most comparative studies on mantle composition and seismic properties discuss methodological errors in some detail, and corresponding error bars are often shown in figures. These errors are expected to decrease with time as methodological constraints improve (Stixrude and Lithgow-Bertelloni, 2005; Stixrude and Lithgow-Bertelloni, 2011; Wu and Wentzcovitch, 2017). Differences in predictions generated by different approaches are often used as a proxy for methodological error, such as the difference between our ab initio pyrolite (blue) and the EoS pyrolite (dashed green) prediction in Fig. 1.

3.1.2. Input error

Input error is specific to the uncertainties in relevant input parameters needed to generate a prediction. For example, unless one knows the temperature precisely at a given location in the interior of the Earth, then it is not possible to generate a precise prediction for the seismic properties of a candidate composition material, and we must account for the range of uncertainty for possible temperatures (and the corresponding influence on seismic properties). If the range of possible temperatures lies between T_1 and T_2, then the predictions for a particular composition must be considered over the entire temperature interval $T_1 \le T \le T_2$. To estimate the input error in this example, we could simply use our predictive model(s) to directly compute:

$$\varepsilon_{pred,input}(P, T, X) = |Y_{pred}(P, T_2, X) - Y_{pred}(P, T_1, X)|. \tag{10}$$

Although this procedure is relatively straightforward, the more challenging task is to choose an appropriate T_1 and T_2, as well as the range of uncertainty in any other important input parameters. Input errors are often not accounted for in comparing predicted elastic properties with seismological models, although as we shall see these are a major source of uncertainty in this context.

3.1.3. Closure error

A fundamental question is whether Y_{earth} and Y_{real} can in principle be compared to one another given the enormous degrees of freedom that are possible at the scales relevant to seismological investigation. For example, while we are forced to assign a characteristic temperature and bulk composition to a parcel of the mantle in order to compare predictions and seismic models, we have no *a priori* constraints on how temperature and composition vary at smaller scales within the volume of interest. In practice, the comparison of Y_{pred} and Y_{mod} must always be made by assuming an appropriate set of "closure conditions" that reduces these vast degrees of freedom to something computationally tractable.

The needed closure conditions usually include a state of thermodynamic equilibrium (or a reasonable approximation thereof), and a restriction to a limited number of influential chemical components. Assuming equilibrium reduces the available degrees of freedom to those dictated by Gibb's phase rule (i.e., the famous $f = c - p + 2$). Local thermodynamic equilibrium may be a reasonable assumption in some circumstances, and is expected over length scales of order $\sim\sqrt{D\tau}$ (where D is the slowest/limiting diffusivity of important chemical species and τ is the elapsed time since the last equilibrium-perturbing event). However, global seismology samples large volumes of rock (up to hundreds of km) that are unlikely to be in thermodynamic equilibrium throughout. When performing comparisons in 1D, the effective seismological sampling volume expands laterally to cover the entire globe, over which we expect significant variations in T and X. Therefore the assumption of thermodynamic equilibrium is not justified at the length scales over which the comparisons are being made, a fact that has already been recognized (but only partly addressed) in the formulation of

"mechanical mixture" models as opposed to "equilibrium models" (Xu et al., 2008; Stixrude and Lithgow-Bertelloni, 2011).

Our ability to make predictions based solely on knowledge of P, T, X also implies that the rock property in question does not depend on other variables, such as size, spatial sorting/distribution, and orientation of grains. These kinds of degrees of freedom are usually suppressed by assuming a state of textural equilibrium and/or random grain orientation, which may also be difficult to justify over length scales relevant to seismic measurements. An example of a way of estimating error bounds associated with physical grain arrangements is the well-known Hashin-Shtrikman interval (Hashin and Shtrikman, 1963). Bounds on uncertainties related to anisotropy could also be estimated straightforwardly by computing estimates for perfectly aligned vs. randomly oriented grains.

Only if all of the closure conditions are met, will we be able to construct an "ideal" scenario in which M_{ideal} could in principle vanish for meaningful input variables for the prediction. However, there will always be some residual uncertainties regarding these assumptions, and they may be difficult to justify using *a priori* constraints.

3.1.4. Parameterization error

Another kind of error is introduced by the manner in which geophysical data are parameterized. For example, in the construction of 1D seismic profiles, one seeks to collapse 3D variations into a single radial profile. This is partly motivated by the fact that seismic velocity variations are dominantly radial, with pressure changes across the mantle having the largest impact on seismic properties and other factors only perturbing the compression-dominated trend by several percent. However, by throwing away lateral variations, the comparisons to be made using Y_{mod} and Y_{pred} also collapse into 1D, and a characteristic P, T, X needs to be assumed at each depth. However, both T and X could vary widely at any given depth, and these variations are crucially important for interpreting and deciphering the internal dynamics of our planet. Such errors might be small if any lateral variations in T and X were normally distributed about the mean value, and the dependence of properties Y upon T and X were dominantly linear in nature. However, this may not always be the case (see Supplementary material for further discussion of this issue).

Global 1D seismic profiles are fitted to a variety of data (see Supplementary material) using different assumptions regarding the attributes of the resulting best-fit curves. The lower mantle of the PREM profile is defined as a cubic expansion of the normalized radius. While the ak135 profile is not similarly defined as a functional form, its slope in the lower mantle can be expressed as cubic segments. Thus, aspects of the data that are not represented by the chosen line fitting properties (the cubic expansion in the case of PREM) will be lost in the resulting 1D profile. These aspects of the data which are smoothed over in the curve fitting process are then no longer available for comparison with the composition models.

3.2. Comparison strategy for discriminatory power

There are many ways that one could approach the application of discriminatory power to comparisons between competing predictions and geophysical constraints. For example, the contribution of errors in scenario i, $M_{err,i}$, could first be estimated based on *a priori* knowledge of all sources of uncertainty, and then applied directly to the comparative analysis. However, the business of "estimating uncertainty" is hazardous, and has many potential pitfalls. Claims of achieving particular error thresholds may be difficult to justify, and such a plan could be susceptible to misapplication or claims of smaller error floors than are plausible in reality. Larger than reasonable error floors, on the other hand, could also be misapplied (e.g., in the construction of a "straw man" argument). In any case, such judgments are often subjective and it would be preferable to follow an approach that allows one to see the trade-offs between uncertainties and discriminatory power directly.

An alternative strategy that leads to greater transparency and better understanding of the relevant trade-offs is to set a target threshold for D_{ij} and then compute the corresponding associated error. For example, one could test 2 composition scenarios, and then use the differences in the predictions to tabulate the maximum permitted uncertainty levels that are needed to satisfy the chosen threshold for D_{ij}. Perhaps an even more practical strategy in this kind of scenario is to plot the error floor for different uncertainties along with the predictions, in order to judge how tightly one needs to constrain the input parameter(s) in order to discriminate between the competing scenarios. This can be performed for chosen threshold values of D_{ij}, or for a variety of different thresholds. We will demonstrate these approaches in the next section.

4. Discriminating lower mantle composition

As noted previously, the largest differences in seismic velocities and densities are predicted to arise between perovskitite and harzburgite composition scenarios, which might be considered to bracket the plausible range of uncertainty in average lower mantle composition. In computing discriminatory power we will use these end-member compositions as examples, to maximize the influence of composition on differences in the comparisons. As such, this example comparison will directly address the question of whether any kind of meaningful predictions regarding lower mantle composition can be made by using mineral physics and 1D seismic models. Pyrolite or other intermediate composition comparisons would generate relatively smaller differences, and therefore require a proportionally smaller error floor to achieve meaningful discriminatory power thresholds.

In the present example we focus on temperature uncertainties that contribute to input errors, which taken alone can be considered to give a lower bound on the total error floor. Later we will argue that temperature is indeed likely to be the greatest contribution to propagated uncertainties in the present context, and the results obtained here will be discussed in light of expected temperature uncertainties in the lower mantle. In computing the discriminatory power we need to define $M_{err,ij}$ in Eq. (8). Here we use the temperature sensitivity of pyrolite composition as representing a middle ground between perovskitite and harzburgite, and is very similar to what one finds by taking the arithmetic mean of the end-member values. This will be used to map sensitivity to temperature uncertainties through to the computation of discriminatory power.

We demonstrate two applications of the discriminatory power approach in Fig. 3. The first application in the top row is the discriminatory power calculated between perovskitite and harzburgite compositions for V_P, V_C, V_S, and ρ for different levels of temperature uncertainty. We considered temperature uncertainties of ± 100, ± 200, ± 300, and ± 400 K. The second application in the middle row of Fig. 3 shows the temperature uncertainty range necessary to achieve a discriminatory power equal to one (the marginal case) and two (the more tenable case). In order to claim that one composition is a better fit to a 1D model than another, it is necessary to justify that the influence of temperature uncertainty at that depth is smaller than the differences in the proposed composition models (i.e., for which $D_{ij} > 1$). To make this more explicit, we plot the numerator of Eq. (7) in the bottom row to show the difference between the two composition models (i.e. perovskitite - harzburgite). We also provide a graphical representation of Eq. (7) in Supplementary Fig. 1.

We find the highest discriminatory power for harzburgite compared to perovskitite for V_P and V_C in the mid-mantle, mostly owing to the softening of the bulk modulus during the iron high-spin to low-spin crossover in ferropericlase (Wentzcovitch et al., 2009). This has a 2-fold effect: first, it enhances the dependence of V_P and V_C upon composition; second, the calculated V_P and V_C have diminished sensitivity to temperature during the spin transition (Wu and Wentzcovitch, 2014). V_S and ρ, on the other hand, yield lower discriminatory power throughout the lower mantle owing to relatively low sensitivity to composition

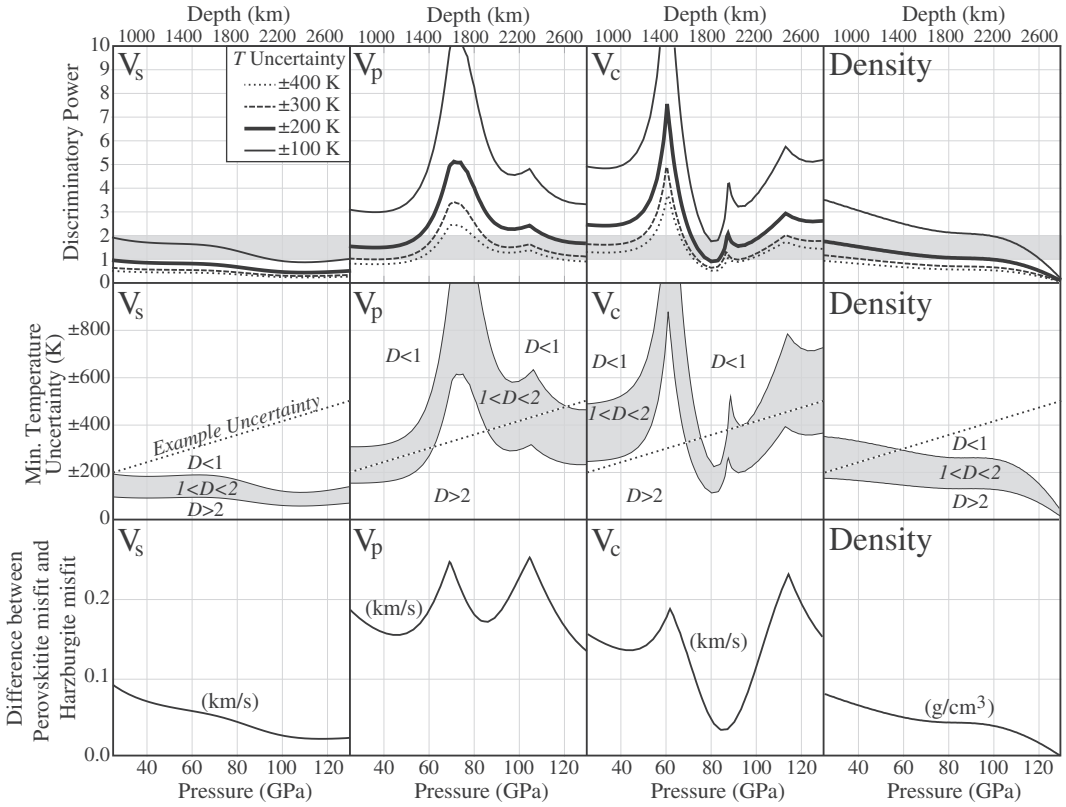

Fig. 3. Top row: Discriminatory power between perovskitite and harzburgite. The discriminatory power maximum occurs in the mid mantle due to the softening of the bulk modulus during the iron high-to-low-spin crossover in ferropericlase (only present in harzburgite). Middle row: The relationship between temperature uncertainty and discriminatory power. We use Eq. (7) to calculate the temperature uncertainty necessary to achieve discriminatory power of 1 and 2, with the region between these two values shaded grey. The dashed line represents a generic (example) temperature uncertainty that gradually increases with depth. The temperature uncertainty permitted for compressional and bulk sound velocity to achieve $D = 2$ is significantly higher than for shear velocity and density. Bottom row: The numerator in the discriminatory power (Eq. (7)), which is the absolute difference between the absolute misfit between harzburgite and PREM and the absolute misfit between perovskitite and PREM. Larger differences in the predictions for different composition scenarios or reduced temperature uncertainty increases the discriminatory power.

relative to modest temperature uncertainties. Note that V_P and V_C also yield a modest discriminatory power in the shallow and deep extremes of the lower mantle.

Over all, we see that V_P and V_C are the most promising quantities for discriminating the kinds of competing mantle composition scenarios examined here. However, this is only true in the depth range 1600–2400 km where the predicted spin transition in ferropericlase amplifies the influence of these variations. This is expected because perovskitite has no ferropericlase, and therefore the manifestation of a spin transition is absent. Harzburgite, on the other hand, is expected to have a moderately large abundance of ferropericlase and the effects of a spin transition are predicted to be strongest for this bulk composition. In the absence of this spin transition, the outcome for V_P and V_C would be similar to the situation for V_S (Wang et al., 2015). Even though the spin transition increases discriminatory power between harzburgite and perovskitite in V_P and V_C, the results show that one still needs to know the temperature of the lower mantle within a precision of ~ ± 200 to 300 K in order for the discriminatory power to become significant. The depth-dependent variation might be more readily distinguished than the values of V_P and V_C alone, however, such patterns are absent in 1D seismic profiles (we discuss this further in the Discussion). In other portions of the lower mantle, V_P, V_S, V_C and ρ have a lower discriminatory power unless one can specify the temperature within ~ ± 150 K. In the next section we will examine sources of error in specifying the temperature of the lower mantle in order to decide whether any of these measures can help us to discriminate lower mantle composition.

5. Estimating temperature uncertainties

Now we consider the conditions for which uncertainties in input temperature are small enough to yield discriminatory power in excess of unity. We illustrate the extent of variability in geotherms for similar compositions for our 3 candidate composition models in Fig. 4. The brown line, which is the coldest on this plot, is the adiabatic geotherm of Brown and Shankland (1981) while the purple line is the super adiabatic geotherm proposed by Anderson (1982). The magenta, blue, and orange lines correspond to the compositions in Table 1. Since EoS methods rely on a predetermined geotherm for extrapolation, Cottaar et al. (2014) found the green line provided a best fit to PREM while Stixrude and Lithgow-Bertelloni (2011) concluded a modified Stacey (1992) geotherm was able to match PREM for a pyrolitic composition. The high temperature estimate of Williams (1998) (olive line) lies just below the upper limits for temperature based on the melting temperature of peridotite compositions (Fiquet et al., 2010; Nomura et al., 2014). The yellow line is the temperature that was considered necessary for perovskitite to fit PREM by Mattern et al. (2005), which is ≈800 K hotter than isentropic geotherms anchored at temperatures compatible with mineralogical phase transitions (Irifune et al., 1998) (see below). On the other hand, our *ab initio* methods previously showed that increasing the temperature for a pure perovskitite by only 500 K at the top of the lower mantle (dark red line) provides a suitable match to PREM (Ballmer et al., 2017).

In the absence of precise knowledge of absolute mantle temperature at each depth, different composition scenarios need not have the same temperatures, and variations in both quantities (or other variable) are

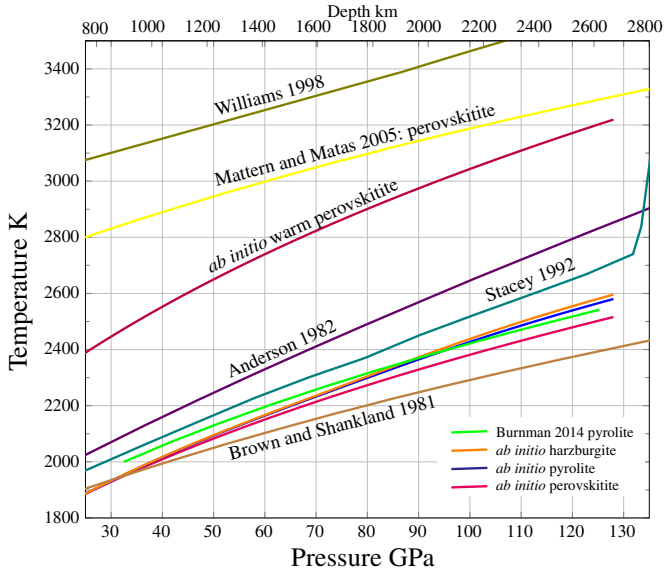

Fig. 4. Proposed geotherms for the lower mantle and those used in this study: magenta for ambient perovskitite, blue for ambient pyrolite, and orange for the ambient harzburgite for which the velocities and density are plotted in Fig. 1. Brown: adiabatic (Brown and Shankland, 1981), purple: super adiabatic (Anderson, 1982), magenta: self-consistent perovskitite, blue: self-consistent pyrolite, orange: self-consistent harzburgite, light green: pyrolite (Cottaar et al., 2014), teal: pyrolite for modified (Stacey, 1992) from (Stixrude and Lithgow-Bertelloni, 2011), olive: high temperature without melt (Williams, 1998), yellow: perovskitite (Mattern et al., 2005), dark red: perovskitite (Ballmer et al., 2017). (For interpretation of the references to colour in this figure, the reader is referred to the web version of this article.)

generally permitted. That is, scenario i could have temperature T_i and composition X_i, while a competing scenario supposes $X_j \neq X_i$ and $T_j \neq T_i$. While both T_i and X_i should be regarded as unknowns, typically temperature is treated as a known quantity. For example, one strategy for selecting a mantle temperature is to use a published "reference geotherm" from the literature for the sake of comparing composition as the only variable. A common choice is the Brown and Shankland geotherm, which was generated from seismic velocity profiles using a simple Debye model (Brown and Shankland, 1981) (Fig. 4, brown line). Note that choosing only a single temperature profile to compare different candidate compositions leads to results that are biased by the choice of temperature. For example, a colder geotherm favors compositions that have greater proportions of seismically slow minerals and likewise, warmer geotherms favor compositions with faster mineralogy. As discussed in the following, the parameters affecting quantities such as adiabatic gradient vary with composition. Therefore, to be fully self-consistent one needs to generate a geotherm whose gradient is compatible with each candidate composition.

Another strategy for estimating lower mantle temperatures is to assume an anchor temperature at a given depth, and then apply an approximation for the temperature gradient to extrapolate to other depths. Temperatures atop the transition zone are moderately well-constrained by the 410 km global seismic discontinuity that is attributed to an olivine-spinel phase transition (Anderson, 1967; Ringwood and Green, 1969; Akaogi et al., 1989; Ita and Stixrude, 1992; Helffrich, 2000). Estimates based on this phase transition, with temperature uncertainties perhaps as small as ~100 K, can be extrapolated to the top of the lower mantle along an adiabat to predict temperatures of around 1873 K at 660 km depth (Irifune et al., 1998). However, the extrapolation across this 250 km depth interval itself strongly depends on assumptions about the dynamics of the transition zone, such as spatially or temporally varying partial layering (Tackley et al., 1993), stagnating slabs (Fukao et al., 2001), the influence of latent heat in several solid-solid phase transitions (Ringwood, 1972), and other possible complexities (Anderson, 2007). Thus extrapolation along an assumed adiabat from 410 km depth pinned by the olivine-spinel transition introduces additional uncertainties for estimates at 660 km depth to ~150 K or more.

While the observed seismic discontinuity at ~660 km depth, attributed to the post-spinel transition (ringwoodite to bridgmanite + periclase), should in principle provide a useful constraint for temperatures atop the lower mantle, the phase boundary is not independently well-constrained. The pressure-temperature dependence of the post-spinel transition is debated. High pressure-temperature experimental constraints on the post-spinel transition rely on the choice of a pressure calibration standard, but unfortunately a variety of available calibrants diverge and do not yield a unique pressure-temperature condition. One proposed solution to this dilemma has been to employ a "geophysically consistent" pressure scale that yields the best agreement with geophysical models and observations (Fei et al., 2004). While this is a practical solution for applying experimental results to geophysics, one cannot also claim that the chosen pressure calibration scale constrains the geotherm because the argument then becomes inherently circular (i.e., a geotherm must be assumed in constructing the scale). In addition, small-scale variations in discontinuity topography (Wu et al., 2019) and lack of an expected anti-correlation of the 410 and 660 km discontinuity topography (Houser and Williams, 2010) suggests a significant competition between temperature and composition to explain the depth of both discontinuities, which further complicates the use of this discontinuity and phase change as a thermometer. Moreover, the estimated phase transition's small Clapeyron slope (i.e., $dP/dT \sim -2$ to -3 MPa/K (Bina and Helffrich, 1994; Akaogi et al., 2007)) results in a weak sensitivity of the phase transition depth to temperature.

Although a temperature anchor in the lowermost mantle would be highly useful for reducing temperature uncertainties, there are considerable challenges in interpreting a potentially complex thermal and chemical boundary layer even before one considers potential geothermometers. If seismic reflections 200–300 km above the core-mantle boundary (CMB) in seismically fast, presumably cold, slab regions are due to the post-perovskite transition (Murakami et al., 2004), then they would represent cooler than average temperatures (Hernlund and Labrosse, 2007) rather than ambient temperatures. There are also significant uncertainties in the temperature of the post-perovskite phase boundary due to potentially large contributions from variations in composition (Hernlund and McNamara, 2015). The temperature at the CMB is not very useful because of large intrinsic uncertainties ($\approx 3800 \pm 400$ K) as well as accounting for the unknown magnitude of the temperature drop across the thermal boundary layer above it (Hernlund and McNamara, 2015).

Once an anchor temperature is established at the top of the lower mantle, the next task is to extrapolate further with depth. It is common to assume an adiabat, since this is the degree to which material heats upon simple compression and therefore the up-down motions of mantle rock should reproduce this basic physical effect to some extent. Lower mantle adiabatic gradients estimated in the literature (Fig. 4) typically fall in the interval 0.3 ± 0.1K/km. However, adopting an adiabatic average profile presupposes a nearly isentropic (well-mixed) dynamical state of the mantle, and in fact this assumption is only strictly applicable to turbulent convection at very high convective vigor (i.e., large Rayleigh number) in a homogeneous fluid. The assumption of lower mantle adiabaticity also relies upon the absence of layering (Anderson, 1982), buoyancy fluctuations (Ballmer et al., 2015), compositional segregation (Kellogg et al., 1999), viscosity hills and jumps (Forte and Mitrovica, 2001; Rudolph et al., 2015), rheological complexities that may prevent mixing to nearly isentropic conditions (Ballmer et al., 2017), inhibitions arising from phase transitions, and so on. The Earth's mantle is influenced by asymmetries associated with spherical shell geometry, internal heating, temperature dependent viscosity, compressibility, and other factors that also cause departures in its

convective style from an idealized simple fluid layer (Schubert et al., 2001). 3D spherical shell mantle convection models that assume a simple fluid rheology, an approximate form of compressibility, and parameters tuned to match temperatures and heat flow in the upper mantle reveal significant departures from adiabaticity in the lower mantle (Zhong, 2006). Therefore extrapolating temperatures to greater depth involves uncertainties in both the adiabatic gradient in addition to the expectation that the lower mantle is not strictly adiabatic. All of these factors contribute to input error for temperatures in the lower mantle.

Another problem is that the dynamical context that produces the geotherm may strongly depend on the chemical composition, owing to feedbacks between composition and transport properties that fundamentally influence mantle dynamics. Mantle temperature has a dynamical dependence on composition due to the influence of chemistry on properties such as the resistance to shear deformation (i.e., effective viscosity) of rocks (Yamazaki and Karato, 2001), variations in compatibilities/concentrations of heat producing elements (Allegre et al., 1983), variations in Grüneisen parameter for different compositions (Stixrude and Lithgow-Bertelloni, 2005), non-linear micro-scale processes resulting from variable modal abundances of aggregates containing multiple phases (Marquardt and Miyagi, 2015), among others. Thus to examine trade-offs between mantle composition and temperature, the feedbacks between composition, long-term mantle rheology, and heat transfer need to be accounted for and better understood.

Applying Tozer's logic (Tozer, 1967), a rock with a composition that is intrinsically rheologically strong would give rise to a hotter geotherm because internal heating (and secular cooling of the core) must balance convected heat loss. An intrinsically more viscous rock composition needs to be maintained at higher temperatures in order to lower the viscosity enough to permit sufficiently vigorous convection that can balance the heat budget. An intrinsically less viscous rock composition, on the other hand, can balance heat flow and production at lower temperatures. Thus, intrinsically more viscous compositions can yield higher temperatures than less viscous counterparts. The effects of composition on rock viscosity are not necessarily correlated with elastic properties, resulting in a myriad of potential trade-offs between mantle dynamics, composition, thermal state, and seismological structure.

The importance of long-term mantle rheology is underscored by the fact that one of the greatest uncertainties in bulk composition of the lower mantle, the Mg/Si ratio, trades off strongly with viscosity because Mg/Si controls the proportion of the strong bridgmanite phase relative to the weak periclase phase. The variation in bulk rock compositions considered in our preceding examples spans a wide range of Mg/Si. Viscosity variations in excess of 3 orders of magnitude might be induced by composition differences in this same Mg/Si range (Yamazaki and Karato, 2001). While it is clear that it is not dynamically self-consistent to choose the same geotherm for a perovskitite composition as for a harzburgitic composition (Valencia-Cardona et al., 2017), the exact degree of the effective viscosity change and requisite temperature compensation in a dynamically evolving complex Earth is not well-constrained.

In summary, to establish a temperature profile in the lower mantle, we face 3 kinds of uncertainty that may contribute to input error. The first is establishing an anchor temperature. The second involves estimating the adiabatic gradient (which is itself comosition-dependent), as well as the extent to which the mantle is not adiabatic. The third source of input error is related to feedbacks between composition and the geotherm that emerge as a consequence of the dependence of transport properties on each scenario. It is clear from these considerations that arriving at a confident estimate for temperature uncertainties is difficult, and ultimately subjective. For this reason, it is better to consider a range of temperature uncertainties and how they trade-off with discriminatory power, as illustrated in the previous section (see also Fig. 3).

6. Discussion

6.1. The pyrolite problem

An adiabatic well-mixed pyrolite-like mantle composition has emerged as a kind of de facto null hypothesis for the lower mantle (see also the discussion in Supplementary material). Since pure bridgmanite velocities are faster and pure ferropericlase velocities are slower than PREM, it may be argued that the lower mantle should be a mixture of the two phases (Ita and Stixrude, 1992; da Silva et al., 2000; Karki et al., 1999, 2001; Wentzcovitch et al., 2004; Mattern et al., 2005; Matas et al., 2007; Stixrude and Lithgow-Bertelloni, 2011; Wu, 2016). The proportion of bridgmanite and ferropericlase that can provide a reasonable fit to PREM (for an assumed adiabatic geotherm) is similar to pyrolite (17% ferropericlase; (Wicks and Duffy, 2016), so it has been proposed that pyrolite best represents the average lower mantle composition (Li and Zhang, 2005; Wang et al., 2015). In addition, some degree of mantle mixing is suggested by seismic tomography images of subducting slabs in the lower mantle (Fukao and Obayashi, 2013) and dynamical models that include deep subduction-driven whole mantle convection and mixing (e.g., van Keken et al., 2002; Deschamps and Tackley, 2009). Thus, pyrolite, representing a well-mixed interior similar to the composition of shallow mantle has emerged as a typical reference lower mantle composition (Maaloe and Aoki, 1977).

Velocity and density values are often shown together on the same plot for brevity, however, this makes it difficult to distinguish between different compositions. Plotted individually, our *ab initio* predictions show that no single composition can simultaneously provide an exact fit to all PREM velocities and density for the same anchor temperature at 660 km depth. Fig. 1 shows that pyrolite, for both the *ab initio* and EoS methods, lies close to PREM although with a different gradient for V_P and V_C. All the compositions have greater V_S than PREM. There is little difference between the densities for all the compositions and they are very close to PREM although perovskitite is slightly denser. The deviations of different compositions from PREM are described in greater detail in Valencia-Cardona et al. (2017). Increasing the iron content in the pyrolite would decrease the velocities but the fit to the density would suffer (as well as mass and moment of inertia of the Earth). Cobden et al. (2009) also found that a uniform composition was not able to match the gradient in PREM. In order to match a pyrolite model to PREM, Cobden et al. (2009) showed that a variable (non-adiabatic) temperature gradient or a change in the bulk composition in the mid-mantle was needed even when applying different equation of state extrapolations and accounting for uncertainties. Thus, it is difficult to justify (adiabatic) pyrolite as the de facto lower mantle composition on the basis of mineral physics and seismology alone.

6.2. Effects of silicon and iron

It should be noted that the Mg/Si of the perovskitite composition is around 0.82 which lies below the value of the Sun ($\approx$1; Palme and O'Neill, 2014). As Mg/Si decreases from our perovskitite composition, SiO_2 phases appear and become more abundant. Silica phases such as stishovite exhibit distinct physical properties and exert a strong influence on seismic velocities even at small fractions in a lower mantle assemblage (Karki et al., 1997; Yang and Wu, 2014; Buchen et al., 2018). It may be difficult to reconcile some composition models with seismic observations. For example, an initial enstatite chondrite composition (Mg/Si $\sim$ 0.8; Javoy et al., 2010) will develop a relatively silica rich lower mantle following the extraction of a peridotitic upper mantle and may not be compatible with observed seismic velocity patterns in the lower mantle.

Owing to its strong effect on density (Irifune et al., 2010; Dorfman and Duffy, 2014), hence mass and moment of inertia, the Fe content of the lower mantle is thought to be relatively well-constrained at $\sim$8% by weight (e.g., McDonough and Sun, 1995). However, the partitioning of

Fe between phases is poorly constrained (Lin et al., 2013). If the influence of Fe/(Mg + Fe) on properties of bridgmanite and ferropericlase were similar, then seismological constraints would be insensitive to Fe-partitioning between the phases and would lack discriminatory power. Note that changes in Fe-partitioning alone do not affect the density of the aggregate unless there is a significant difference between the partial molar volume of Fe relative to Mg. On the other hand, the fraction of Fe in ferropericlase does exert an influence on the bulk modulus and density owing to the spin crossover, while Fe in bridgmanite does not exert the same effects at the same conditions.

6.3. Ferropericlase spin crossover

We find that the discriminatory power is greatest for V_P around pressures of 90 GPa when comparing compositions with varying Mg/Si, owing to the Fe spin crossover in ferropericlase (a phase that increases in abundance with increasing Mg/Si) (Figs. 2 and 3). The implication is that the spin crossover may provide an opportunity to constrain lower mantle Mg/Si.

Our *ab initio* method incorporates the vibrational contribution to the free energy using linear response theory (Baroni et al., 2001; Wentzcovitch et al., 2009) which recovers a softening of the bulk modulus during the high-to-low spin crossover that agrees with experimental studies (Marquardt et al., 2018). The resulting downward inflection in the V_P profile through the mid-lower mantle that arises due to softening of the bulk modulus in iron bearing ferropericlase is not a feature in 1D seismic models. As mentioned in Section 3.1.4, such inflections may be present in global seismic data, but are lost in the curve fitting process. Updating global seismic travel time catalogs could reveal mid-mantle inflections. The depth range of the spin crossover is temperature dependent (Wentzcovitch et al., 2009) such that it would be necessary to examine the entire lower mantle and compare results from regional profiles in order to determine if there is any signal in 1D seismic travel times.

Assuming that our *ab initio* calculations are correct, there are several possibilities that warrant further consideration. Option 1: the amount of ferropericlase is below the threshold for detection (i.e., low Mg/Si). Option 2: ferropericlase is heterogeneously distributed in a way that does not manifest in the 1D profiles. Option 3: the effects of ferropericlase are masked by coincident variations in temperature and composition. Option 4: iron strongly partitions into bridgmanite in the depth range where the spin crossover occurs. The complete absence of ferropericlase in 1D lower mantle seismic profiles might be difficult to reconcile with the presence of at least some degree of circulation and mixing between the shallow and deep mantle. Exploring the other options warrants further study.

A depression in the geotherm and/or Mg/Si at mid-mantle depths could dampen the signature of the iron spin crossover in ferropericlase. For example, cooler temperatures could arise at mid-mantle depth if there exists an abnormally large amount of subducting slabs in this region (the present mantle is only a snapshot in geological time). However, subducted slabs lithosphere is dominantly depleted harzburgitic material that is expected to have a higher Mg/Si (i.e., enriched in ferropericlase). A decrease in Mg/Si is also consistent with the BEAMS model (Ballmer et al., 2017), in which highly viscous silica-rich rocks accumulate at the cores of convection cells in the mid-lower mantle, possibly anchoring the pattern of deep mantle convection (Dziewonski et al., 2010). The BEAMS scenario could be tested by examining whether signatures of the spin crossover manifest in regions where subducting lithosphere is expected to be present, and absent in ambient mantle domains.

6.4. Future directions

While the results obtained here cast doubt on our ability to discriminate lower mantle composition using 1D seismic models and mineral physics predictions alone, there are many potential strategies that could overcome these weaknesses. Here we discuss a few possibilities to motivate further research on this topic and the development of new methods/approaches.

The main issue we highlighted in the lower mantle is a relatively low sensitivity of seismic properties to bulk composition compared to the sensitivity to temperature variations (combined with uncertainty in the latter). The situation is reversed for the Earth's outer core, where sound speed is insensitive to temperature (Vočadlo et al., 2003) but highly sensitive to changes in composition (Hirose et al., 2013). In this circumstance, major breakthroughs in determining core composition might help to balance the composition of the entire Earth, allowing us to test ideas such as whether the core hosts a large proportion of silicon, thereby allowing for a higher Mg/Si mantle in order to sustain chondritic and solar abundances. Still the seismological observations have a role to play because such proposals also must be weighed against the lack of any obvious signature of a Fe spin crossover in ferropericlase that would be expected in that case. In this sense, propositions about composition in one region can be weighed against predictions for seismic properties in another, allowing us to leverage more constraints.

Mantle composition is intrinsically linked to the history of accretion, core segregation, and billions of years of mantle evolution. Particular choices of composition are therefore linked to particular hypotheses about how the Earth formed and evolved. Certain choices of composition also influence other properties, such as the effective viscosity of rocks at lower mantle conditions, which is thought to be highly sensitive to Mg/Si (Yamazaki and Karato, 2001) or electrical conductivity (Khan et al., 2008). Approaches seeking to find links between lower mantle composition and dynamics (e.g., Kellogg, 1993; Jordan et al., 1993; Kellogg et al., 1999; Deschamps and Trampert, 2003; Matas et al., 2007; Khan et al., 2008; Cobden et al., 2009; Styles et al., 2011; Cammarano et al., 2011; Davies et al., 2012; Nakagawa et al., 2012; Tosi et al., 2013) offer important constraints. Variations in composition may also affect phase transitions, relative densities of rocks and propensity for layering, and many other related issues. Finally, linking major element composition models and evolution scenarios to isotopic evidence and petrological constraints is key to identifying the source region(s) of observed anomalies and linking those to a coherent chemical and physical model.

While many of the shortcomings we identified above were discussed in the context of 1D seismic profiles, we are hopeful that both regional models as well as 3D variations in the Earth can offer a promising avenue for deciphering composition (and any variations) in the lower mantle. Testing mineral physics results against regional seismic profiles requires diverse tectonic environments, which will be facilitated by new seismic networks and growth of existing networks. The Reference Earth Model 3D project, aims to develop a 3D model that is a synthesis of data contributed by a wide swath of the seismology community (https://www.geol.umd.edu/facilities/seismology/rem-3d/). Ideally it would be possible to evaluate the error on the resulting models which we argue is essential when comparing to mineral physics results. Another effort is the Collaborative Seismic Earth Model (CSEM-1) described by Fichtner et al. (2018) that provides access to data and inversion schemes that can handle the variable resolution of combining multiscale datasets. Additionally, tools are emerging to evalute the large suite of tomographic models that are currently available. Lekic et al. (2012) examined regional 1D models by clustering of 3D tomography models and Cottaar and Lekic (2016) who combine tomography models to investigate large low shear velocity province morphology. The “vote map” method introduced by Shephard et al. (2017) available on the (https://www.earth.ox.ac.uk/smachine/cgi/index.php) platform enables interrogation of coherent structure in tomography models.

Another approach is to target particular regions for comparative study. For example, (Deschamps et al., 2019) illustrate the type of approach necessary to make progress in characterizing composition variations in the lowermost mantle. They collect and combine different

types of seismic data (travel times and amplitudes) to have independent constraints on temperature and take into account a whole suite of uncertainties in their assumptions. They state that their temperature uncertainty is ± 500 K for their analysis and still found a signal in the western Pacific consistent with an increase in iron relative to the surrounding mantle which they are not able to identify at a similarly resolved portion of the northern Pacific (given the errors). Likewise, there is an abundance of studies that incorporate anisotropy and attenuation as additional constraints to overcome the temperature/composition ambiguity with recent examples including Ferreira et al. (2019) and Euler and Wysession (2017). Thus, there is still much to be distilled from seismic interrogation of lower mantle properties even when accounting for the uncertainties inherent to investigating this remote region of our planet.

7. Conclusions

The purpose of this study is not to argue for any particular composition or thermal model, but to examine the use of global 1D average seismic models to constrain the composition of the lower mantle. We develop a measure of discriminatory power which compares the magnitudes of the comparative fit between composition model predictions with the associated uncertainties. We demonstrate that while the seismic velocities and densities of compositions with varying proportions of ferropericlase and bridgmanite converge as depth increases in the lowermost mantle, the temperature uncertainty increases. One of these effects alone would hinder our ability to discriminate between different compositions, but together they pose a great obstacle to 1D seismic model fitting. However, in the mid mantle, the high-to-low spin crossover in iron may provide a means to constrain ferropericlase abundance. The complex relations/trade offs between composition, temperature, and dynamics require further investigation and the discriminatory power approach is designed to guide future comparisons between 1D profiles of geophysical models, observations, and predictions.

Credit authorship contribution statement

C. Houser:Conceptualization, Investigation, Writing - original draft.**J.W. Hernlund**:Conceptualization, Investigation, Writing - original draft.**J. Valencia-Cardona**:Formal analysis.**R.M. Wentzcovitch**:Investigation, Formal analysis, Writing - original draft.

Declaration of competing interest

There is no conflict of interest.

Acknowledgments

We appreciate the comments of 5 anonymous reviewers which greatly improved this manuscript. C.H. and J.W.H. were primarily supported by the WPI-funded Earth-Life Science Institute at Tokyo Institute of Technology as well as additional support through JSPS KAKENHI grant numbers 15H05832, 16H06285, and 19K04035. R.M.W. and J.V-C. were funded through NSF grants EAR-1319361 and EAR-1348066.

Appendix A. Supplementary data

Supplementary data to this article can be found online at https://doi.org/10.1016/j.pepi.2020.106552.

References

Akaogi, M., Ito, E., Navrotsky, A., 1989. Olivine-modified spinel-spinel transitions in the system Mg_2SiO_4 – Fe_2SiO_4: calorimetric measurements, thermochemical calculation, and geophysical application. J. Geophys. Res. 94, 15671–15685.

Akaogi, M., Takayama, H., Kojitani, H., Kawaji, H., Atake, T., 2007. Low-temperature heat capacities, entropies and enthalpies of Mg_2SiO_4 polymorphs, and α-β-γ and post-spinel phase relations at high pressure. Phys. Chem. Minerals 34, 169–183. https://doi.org/10.1007/s00269–006–0137–3.

Allegre, C.J., Staudacher, T., Sarda, P., Kurz, M., 1983. Constraints on the evolution of Earth's mantle from rare gas systematics. Nature 303, 762–766.

Allegre, C.J., Poirier, J., Humler, E., Hofmann, A.W., 1995. The chemical composition of the Earth. Earth Planet. Sci. Lett. 134, 515–526.

Anderson, D.L., 1967. Phase changes in the upper mantle. Science 157, 1165–1173.

Anderson, O.L., 1982. The Earth's core and the phase diagram of iron. Phil. Trans. R. Soc. Lond. 306, 21–35.

Anderson, D., 2007. The Eclogite Engine: Chemical Geodynamics As a Galileo Thermometer. Plates, Plumes and Planetary Processes. Geological Society of America, In.

Badro, J., Brodholt, J.P., Piet, H., Siebert, J., Ryerson, F.J., 2015. Core formation and core composition from coupled geochemical and geophysical constraints. Pro. Nat. Aca. Science 112, 12310–12314.

Baker, M.B., Beckett, J.R., 1999. The origin of abyssal peridotites: a reinterpretation of constraints based on primary bulk compositions. Earth Planet. Sci. Lett. 171, 49–61.

Ballmer, M.D., Schmerr, N.C., Nakagawa, T., Ritsema, J., 2015. Compositional mantle layering revealed by slab stagnation at ~1,000 km depth. Sci. Adv. 1, e1500815.

Ballmer, M.D., Houser, C., Hernlund, J.W., Wentzcovitch, R.M., Hirose, K., 2017. Persistence of strong silica-enriched domains in the Earth's lower mantle. Nat. Geosci. 10, 236–241.

Baroni, S., de Gironcoli, S., Corso, A.D., Giannozzi, P., 2001. Phonons and related crystal properties from density-functional perturbation theory. Rev. Mod. Phys. 73 (2), 515–562.

Bina, C., Helffrich, G., 1994. Phase transition Clapeyron slopes and transition zone seismic discontinuity topography. J. Geophys. Res. 99, 15853–15860.

Brown, J.M., Shankland, T.J., 1981. Thermodynamic parameters in the Earth as determined from seismic profiles. Geophys. J. R. Astron. Soc. 66, 579–596.

Buchen, J., Marquardt, H., Schulze, K., Speziale, S., Ballaran, T.B., Nishiyama, N., Hanfland, M., 2018. Equation of state of polycrystalline stishovite across the tetragonal-orthorhombic phase transition. J. Geophys. Res. 123, 7347–7360.

Cammarano, F., Goes, S., Deuss, A., Giardini, D., 2005. Is a pyrolitic adiabatic mantle compatible with seismic data? Earth Planet Sci. Lett. 232, 227–243.

Cammarano, F., Tackley, P., Boschi, L., 2011. Seismic, petrological and geodynamical constraints on thermal and compositional structure of the upper mantle: global thermo-chemical models. Geophys. J. Int. 187, 1301–1318.

Caracas, R., Wentzcovitch, R.M., Price, G.D., Brodholt, J., 2005. $CaSiO_3$ perovskite at lower mantle pressures. Geophys. Res. Lett. 32, L06306.

Carrier, P., Wentzcovitch, R.M., Tsuchiya, J., 2007. First-principles prediction of crystal structures at high temperatures using the quasiharmonic approximation. Phys. Rev. B 76 (6).

Catalli, K., Shim, S.-H., Prakapenka, V.B., Zhao, J., Sturhahn, W., Chow, P., et al., 2010. Spin state of ferric iron in $MgSiO_3$ perovskite and its effect on elastic properties. Earth Planet. Sci. Lett. 289 (1–2), 68–75.

Cawood, P.A., Kroner, A., Pisarevsky, S., 2006. Precambrian plate tectonics: criteria and evidence. GSA Today 16, 4–11.

Ceperley, D.M., Alder, B.J., 1980. Ground state of the electron gas by a stochastic method. Phys. Rev. Lett. 45.

Cobden, L., Goes, S., Ravenna, M., Styles, E., Cammarano, F., Gallagher, K., Connolly, J.A.D., 2009. Thermochemical interpretation of 1-D seismic data for the lower mantle: the significance of nonadiabatic thermal gradients and compositional heterogeneity. J. Geophys. Res. 114. https://doi.org/10.1029/2008JB006262.

Cococcioni, M., de Gironcoli, S., 2005. Linear response approach to the calculation of the effective interaction parameters in the LDA + U method. Phys. Rev. B 71 (3).

Connolly, J.A.D., 2009. The geodynamic equation of state: what and how. Geochem. Geophys. Geosyst. 10, Q10014.

Connolly, J.A.D., Khan, A., 2016. Uncertainty of mantle geophysical properties computed from phase equilibrium models. Geophys. Res. Lett. 43, 5026–5034.

Cottaar, S., Lekic, V., 2016. Morphology of seismically slow lower-mantle structures. Geophys. J. Int. 207 (2), 1122–1136.

Cottaar, S., Heister, T., Rose, I., Unterborn, C., 2014. BurnMan: a lower mantle mineral physics toolkit. Geochem. Geophys. Geosyst. 15 (4), 1164–1179.

da Silva, C., Wentzcovitch, R., Patel, A., Price, G., Karato, S., 2000. The composition and geotherm of the lower mantle: constraints from the calculated elasticity of silicate perovskite. Phys. Earth Planet. Int. 118, 103–109.

Davies, D.R., Goes, S., Davies, J.H., Schuberth, B.S.A., Bunge, H.-P., Ritsema, J., 2012. Reconciling dynamic and seismic models of Earth's lower mantle: the dominant role of thermal heterogeneity. Earth Planet. Sci. Lett. 353, 253–269.

Deschamps, F., Tackley, P.J., 2008. Searching for models of thermo-chemical convection that explain probabilistic tomography I - principles and influence of rheological parameters. Phys. Earth. Planet. Int. 171, 357–373.

Deschamps, F., Tackley, P.J., 2009. Searching for models of thermo-chemical convection that explain probabilistic tomography II - influence of physical and compositional parameters. Phys. Earth. Planet. Int. 176, 1–18.

Deschamps, F., Trampert, J., 2003. Mantle tomography and its relation to temperature and composition. Phys. Earth. Planet Int. 140, 277–291.

Deschamps, F., Cobden, L., Tackley, P.J., 2012. The primitive nature of large low shear-

wave velocity provinces. Earth Planet. Sci. Lett. 349–350, 198–208.
Deschamps, F., Konishi, K., Fuji, N., Cobden, L., 2019. Radial thermo-chemical structure beneath Western and Northern Pacific from seismic waveform inversion. Earth Planet. Sci. Lett. 520, 153–163.
Dorfman, S.M., Duffy, T.S., 2014. Effect of Fe-enrichment on seismic properties of perovskite and post-perovskite in the deep lower mantle. Geophys. J. Int. 197, 910–919.
Dziewonski, A.M., Anderson, D.L., 1981. Preliminary reference Earth model. Phys. Earth Planet. Inter. 25, 297–356.
Dziewonski, A., Lekic, V., Romanowicz, B., 2010. Mantle anchor structure: an argument for bottom up tectonics. Earth Planet. Sci. Lett. 299 (1–2), 69–79.
Euler, G., Wysession, M.E., 2017. Geographic variations in lowermost mantle structure from the ray parameters and decay constants of core-diffracted waves. J. Geophys. Res. 122, 5369–5394.
Fei, Y., Van Orman, J., Li, J., van Westrenen, W., Sanloup, C., Minarik, W., Hirose, K., Komabayashi, T., Walter, M., Funakoshi, K., 2004. Experimentally determined postspinel transformation boundary in Mg_2SiO_4 using MgO as an internal pressure standard and its geophysical implications. J. Geophys. Res. 109, B02305.
Ferreira, A. M. G., Faccenda, M., Sturgeon, W., Chang, S.-J., Schardong, L., 2019. Ubiquitous lower-mantle anisotropy beneath subduction zones. Nat. Geo. 12, 301Ð306.
Fichtner, A., van Herwaarden, D.-P., Afanasiev, M., Simute, S., Krischer, L., Y., C.-S., et al., 2018. The Collaborative Seismic Earth Model: generation 1. Geophys. Res. Lett. 45, 4007–4016.
Fiquet, G., Auzuende, A.L., Siebert, J., Corgne, A., Bureau, H., Ozawa, H., Garbarino, G., 2010. Melting of peridotite to 140 Gigapascals. Science 329, 1516–1518.
Floris, A., de Gironcoli, S., Gross, E.K.U., Cococcioni, M., 2011. Vibrational properties of MnO and NiO from DFT plus U-based density functional perturbation theory. Phys. Rev. B 84 (16).
Forte, A.M., Mitrovica, J.X., 2001. Deep-mantle high-viscosity flow and thermochemical structure inferred from seismic and geodynamic data. Nature 410, 1049–1056.
Fu, S., Yang, J., Zhang, Y., Okuchi, T., McCammon, C. A., Kim, H., Lee, S., Lin, J., 2018. Abnormal elasticity of Fe-bearing bridgmanite in the Earth's lower mantle. Geophys. Res. Lett. 45, 4725–4732.
Fukao, Y., Obayashi, M., 2013. Subducted slabs stagnant above, penetrating through, and trapped below the 660 km discontinuity. J. Geophys. Res. 118, 5920–5938.
Fukao, Y., Widiyantoro, S., Obayashi, M., 2001. Stagnant slabs in the upper and lower mantle transition region. Rev. Geophys. 39, 291–323.
Fukao, Y., Obayashi, M., Nakakuki, T., et al., 2009. Stagnant slab: a review. Annu. Rev. Earth Planet. Sci. 37, 19–46.
Garnero, E.J., McNamara, A.K., Shim, S.-H., 2016. Continent-sized anomalous zones with low seismic velocity at the base of Earth's mantle. Nat. Geosci. 9, 481–489.
Hashin, Z., Shtrikman, S., 1963. A variational approach to the theory of elastic behavior of multiphase materials. J. Mech. Phys. Solids 11, 127–140.
Helffrich, G., 2000. Topography of the transition zone seismic discontinuities. Rev. Geophys. 38, 141–158.
Hernlund, J.W., Houser, C., 2008. On the distribution of seismic velocities in Earth's deep mantle. Earth Planet. Sci. Lett. 265, 423–437.
Hernlund, J.W., Labrosse, S., 2007. Geophysically consistent values of the perovskite to post-perovskite transition Clapeyron slope. Geophys. Res. Lett. 34, L05309.
Hernlund, J. W., McNamara, A. K., 2015. The core-mantle boundary region. In: Schubert, G., Bercovici, D. (Eds.), Treatise on Geophyiscs, vol. 7. Elsevier, pp. 461–519.
Hirose, K., Labrosse, S., Hernlund, J., 2013. Composition and state of the core. Annu. Rev. Earth Planet. Sci. 41, 657–691.
Hofmann, A.W., 1997. Mantle geochemistry: the message from oceanic volcanism. Nature 385, 219–229.
Houser, C., Williams, Q., 2009. The relative wavelengths of fast and slow velocity anomalies in the lower mantle: contrary to the expectations of dynamics? Phys. Earth Planet. Int. 176, 187–197.
Houser, C., Williams, Q., 2010. Reconciling Pacific 410 and 660 km discontinuity topography, transition zone shear velocity patterns, and mantle phase transitions. Earth Planet. Sci. Lett. 296, 255–266.
Houser, C., Masters, G., Shearer, P., Laske, G., 2008. Shear and compressional velocity models of the mantle from cluster analysis of long-period waveforms. Geophys. J. Int. 174, 195–212.
Hsu, H., Wentzcovitch, R.M., 2014. First-principles study of intermediate-spin ferrous iron in the Earth's lower mantle. Phys. Rev. B 90 (19).
Hsu, H., Umemoto, K., Cococcioni, M., Wentzcovitch, R.M., 2009. First-principles study for low-spin LaCoO3 with a structurally consistent Hubbard U. Phys. Rev. B 79 (12).
Hsu, H., Blaha, P., Cococcioni, M., Wentzcovitch, R., 2011. Spin-state crossover and hyperfine interactions of ferric iron in $MgSiO_3$ perovskite. Phys. Rev. Lett. 106.
Hsu, H., Yu, Y.G.G., Wentzcovitch, R.M., 2012. Spin crossover of iron in aluminous $MgSiO_3$ perovskite and post-perovskite. Earth Planet. Sci. Lett. 359, 34–39.
Irifune, T., Nishiyama, N., Kuroda, K., Inoue, T., Isshiki, M., Utsumi, W., Funakoshi, K., Urakawa, S., Uchica, T., Katsura, T., Ohtaka, O., 1998. The postspinel phase boundary in Mg_2SiO_4 determined by in situ X-ray diffraction. Science 279, 1698–1700.
Irifune, T., Shinmei, T., McCammon, C.A., Miyajima, N., Rubie, D.C., Frost, D.J., 2010. Iron partitioning and density changes of pyrolite in Earth's lower mantle. Science 327, 193Ð195.
Ita, J., Stixrude, L., 1992. Petrology, elasticity, and composition of the mantle transition zone. J. Geophys. Res. 97, 6849–6866.
Javoy, M., Kaminski, E., Guyot, F., Andrault, D., Sanloup, C., Moreira, M., Labrosse, S., Jambon, A., Agrinier, P., Davaille, A., Jaupart, C., 2010. The Chemical Composition of the Earth: Enstatite Chondrite Models 293, 259–268.
Jordan, T., Puster, P., Glatzmaier, G., Tackley, P., 1993. Comparisons between seismic Earth structures and mantle flow models based on radial correlation functions. Science 261, 1427Ð1431.
Karki, B.B., Stixrude, L., Crain, J., 1997. Ab inito elasticity of three high-pressure polymorphs of silica. Geophys. Res. Lett. 24, 3269–3272.
Karki, B.B., Wentzcovitch, R.M., de Gironcoli, S., Baroni, S., 1999. First-principles determination of elastic anisotropy and wave velocities of MgO at lower mantle conditions. Science 286, 1705–1707.
Karki, B.B., Wentzcovitch, R.M., de Gironcoli, S., Baroni, S., 2001. First principles thermoelasticity of $MgSiO_3$-perovskite: consequences for the inferred properties of the lower mantle. Geophys. Res. Lett. 28, 2699.
Kawai, K., Tsuchiya, T., 2014. P-V-T equation of state of cubic $CaSiO_3$ perovskite from first-principles computation. J. Geophys. Res. 119, 2801–2809.
Kawai, K., Tsuchiya, T., 2015. Small shear modulus of cubic $CaSiO_3$ perovskite. Geophys. Res. Lett. 42, 2718Ð2726.
Kellogg, L. H., 1993. Chaotic mixing in the Earth's mantle. In: Dmowska, R., Saltzman, B. (Eds.), Advances in Geophysics. Vol. 34. Academic Press, pp. 1–33.
Kellogg, L.H., Hager, B.H., van der Hilst, R., 1999. Compositional stratification in the deep mantle. Science 283, 1881Ð1884.
Kennett, B., Engdahl, E.R., Buland, R., 1995. Constraints on seismic velocities in the Earth from travel times. Geophys. J. Int. 122, 108–124.
Khan, A., Connolly, J.A.D., Taylor, S., 2008. Inversion of seismic and geodetic data for the major element chemistry and temperature of the Earth's mantle. J. Geophys. Res. 113 (B9).
Kulik, H.J., Cococcioni, M., Scherlis, D.A., Marzari, N., 2006. Density functional theory in transition-metal chemistry: a self-consistent Hubbard U approach. Phys. Rev. Lett. 97 (10).
Lekic, V., Cottaar, S., Dziewonski, A., Romanowicz, B., 2012. Cluster analysis of global lower mantle tomography: a new class of structure and implications for chemical heterogeneity. Earth Planet. Sci. Lett. 357Ð358, 68Ð77.
Li, B., Zhang, J., 2005. Pressure and temperature dependence of elastic wave velocity of $MgSiO_3$ perovskite and the composition of the lower mantle. Phys. Earth Planet. Int. 151, 143–154.
Lin, J.-F., Alp, E.E., Mao, Z., Inoue, T., McCammon, C.A., Xia, Y.M., Chow, P., Zhao, J.Y., 2012. Electronic spin states of ferric and ferrous iron in the lower-mantle silicate perovskite. Am. Mineral. 97, 592–597.
Lin, J.-F., Speziale, S., Mao, Z., Marquardt, H., 2013. Effects of the electronic spin transitions of iron in lower mantle minerals: implications for deep mantle geophysics and geochemistry. Rev. Geophys. 51, 244–275.
Lin, J.-F., Mao, Z., Yang, J., Liu, J., Xiao, Y., Chow, P., Okuchi, T., 2016. High-spin Fe^{2+} and Fe^{3+} in single-crystal aluminous bridgmanite in the lower mantle. Geophys. Res. Lett. 43, 6952–6959.
Maaloe, S., Aoki, K., 1977. The major element composition of the upper mantle estimated from the composition of lherzolites. Contrib. Mineral. Petrol. 63, 161–173.
Mao, Z., Lin, J.-F., Yang, J., Inoue, T., Prakapenka, V.B., 2015. Effects of the Fe^{3+} spin transition on the equation of state of bridgmanite. Geophys. Res. Lett. 42, 4335–4342.
Marcondes, M.L., Zhang, F., Wentzcovitch, R.M., 2019. Vibrational Properties of Ferropericlase Across the Iron Spin-crossover. (in prepration).
Marquardt, H., Miyagi, L., 2015. Slab stagnation in the shallow lower mantle linked to an increase in mantle viscosity. Nat. Geosci. 8, 311–314.
Marquardt, H., Buchen, J., Mendez, A., Kurnosov, A., Wendt, M., Rothkirch, A., Pennicard, D., Liermann, H., 2018. Elastic softening of $(Mg_{0.8}Fe_{0.2})O$ ferropericlase across the iron spin crossover measured at seismic frequencies. Geophys. Res. Lett. 45, 6862–6868.
Matas, J., Bass, J., Ricard, Y., Mattern, E., Bukowinski, M.S.T., 2007. On the bulk composition of the lower mantle: predictions and limitations from generalized inversion of radial seismic profiles. Geophys. J. Int. 170, 764–780.
Mattern, E., Matas, J., Ricard, Y., Bass, J., 2005. Lower mantle composition and temperature from mineral physics and thermodynamic modelling. Geophys. J. Int. 160, 973–990.
McDonough, W.F., Sun, S., 1995. The composition of the Earth. Chem. Geol. 120, 223–253.
Mosca, I., Cobden, L., Deuss, A., Ritsema, J., Trampert, J., 2012. Seismic and mineralogical structures of the lower mantle from probabilistic tomography. J. Geophys. Res. 117, B06304.
Mukhopadhyay, S., 2012. Early differentiation and volatile accretion recorded in deep-mantle neon and xenon. Nature 486 (7401), 101–104.
Mundl, A., Touboul, M., Jackson, M.G., Day, J.M., Kurz, M.D., Lekic, V., Helz, R.T., Walker, R.J., 2017. Tungsten-182 heterogeneity in modern ocean island basalts. Science 356, 66–69.
Murakami, M., Hirose, K., Sata, N., Ohishi, Y., Kawamura, K., 2004. Phase transition of $MgSiO_3$ perovskite in the deep lower mantle. Science 304, 855–858.
Nakagawa, T., Tackley, P. J., Deschamps, F., Connolly, J. A., 2012. Radial 1-D seismic structures in the deep mantle in mantle convection simulations with self-consistently calculated mineralogy. Geochem. Geophys. Geosyst. 13(11).
Nestola, F., Korolev, N., Kopylova, M., Rotiroti, N., Pearson, D.G., Pamato, M.G., Alvaro, M., Peruzzo, L., Gurney, J.J., Moore, A.E., Davidson, J., 2018. $CaSiO_3$ perovskite in diamond indicates the recycling of oceanic crust into the lower mantle. Nature 555, 237–241.
Nomura, R., Hirose, K., Uesugi, K., Ohishi, Y., Tsuchiyama, A., Miyake, A., Ueno, Y., 2014. Low core-mantle boundary temperature inferred from the solidus of pyrolite. Science 343, 522–525.
Oganov, A.R., Ono, S., 2004. Theoretical and experimental evidence for a post-perovskite phase of $MgSiO_3$ in Earth's D″ layer. Nature 430, 445–448.
Ozawa, H., Hirose, K., Yonemitsu, K., Ohishi, Y., 2016. High-pressure melting experiments on FeÐSi alloys and implications for silicon as a light element in the core. Earth Planet. Sci. Lett. 456, 47–54.
Palme, H., O'Neill, H., 2014. Cosmochemical estimates of mantle composition. In:

Holland, H., Turekian, K. (Eds.), Treatise on Geochemistry, 2nd Edition. Elsevier, pp. 1–39.
Pearson, D.G., Brenker, F.E., Nestola, F., McNeill, J., Nasdala, L., Hutchison, M.T., Matveev, S., Mather, K., Silversmit, G., Schmitza, S., Vekemans, B., Vincze, L., 2014. Hydrous mantle transition zone indicated by ringwoodite included within diamond. Nature 507, 221–224.
Piet, H., Badro, J., Nabiei, F., Dennenwaldt, T., Shim, S.-H., Cantoni, M., HŽbert, C., Gillet, P., 2016. Spin and valence dependence of iron partitioning in Earth's deep mantle. Proc. Nat. Acad. Sci. 113 (40), 11,127–11,130.
Resovsky, J., Trampert, J., van der Hilst, R.D., 2005. Error bars for the global seismic Q profile. Earth Planet. Sci. Lett. 230, 413–423.
Ringwood, A.E., 1962. A model for the upper mantle. J. Geophys. Res. 67, 857–867.
Ringwood, A.E., 1972. Phase transformations and mantle dynamics. Earth Planet. Sci. Lett. 14, 233–241.
Ringwood, A. E., Green, D. H., 1969. Phase transitions. In: Hart, P. J. (Ed.), The Earth's Crust and Upper Mantle, Volume 13. American Geophysical Union, pp. 637–649.
Rubie, D. C., Jacobson, S. A., 2016. Mechanisms and geochemical models of core formation. In: Terasaki, H., Fischer, R. A. (Eds.), Deep Earth: Physics and Chemistry of the Lower Mantle and Core. Wiley, pp. 181–190.
Rudolph, M., Lekic, V., Lithgow-Bertelloni, C., 2015. Viscosity jump in Earth's mid-mantle. Science 350, 1349–1352.
Schubert, G., Turcotte, D.L., Olson, P., 2001. Mantle Convection in the Earth and Planets, 1st edition. Cambridge University Press.
Shephard, G.E., Matthews, K.J., Hosseini, K., Domeier, M., 2017. On the consistency of seismically imaged lower mantle slabs. Sci. Rep. 7, 10976.
Shukla, G., Wu, Z., Hsu, H., Floris, A., Cococcioni, M., Wentzcovitch, R.M., 2015. Thermoelasticity of Fe^{2+}-bearing bridgmanite. Geophys. Res. Lett. 42, 1741–1749.
Shukla, G., Cococcioni, M., Wentzcovitch, R.M., 2016. Thermoelasticity of Fe^{3+}- and Al-bearing bridgmanite: effects of iron spin crossover. Geophys. Res. Lett. 43, 5661–5670.
Stacey, F., 1992. Physics of the Earth, Volume 1. Brookfield Press.
Stixrude, L., Lithgow-Bertelloni, C., 2005. Thermodynamics of mantle minerals - I. Physical properties. Geophys. J. Int. 162, 610–632.
Stixrude, L., Lithgow-Bertelloni, C., 2011. Thermodynamics of mantle minerals II, phase equilibria. Geophys. J. Int. 184, 1180–1213.
Styles, E., Davies, D.R., Goes, S., 2011. Mapping spherical seismic into physical structure: biases from 3-D phase-transition and thermal boundary-layer heterogeneity. Geophys. J. Int. 184, 1371–1378.
Tackley, P.J., Stevenson, D.J., Glatzmaier, G.A., Schubert, G., 1993. Effects of an endothermic phase transition at 670 km depth in a spherical model of convection in the Earth's mantle. Nature 361, 699–704.
Tosi, N., Yuen, D.A., de Koker, N., Wentzcovitch, R.M., 2013. Mantle dynamics with pressure- and temperature-dependent thermal expansivity and conductivity. Phys. Earth Planet. Inter. 217, 48–58.
Tozer, D.C., 1967. Some aspects of thermal convection theory for the Earth's mantle. Geophys. J. Royal Astronom. Soc. 14 (1–4), 395–402.
Trampert, J., Vacher, P., Vlaar, N., 2001. Sensitivities of seismic velocities to temperature, pressure and composition in the lower mantle. Phys. Earth Planet. Int. 124, 255–267.
Trampert, J., Deschamps, F., Resovsky, J., Yuen, D.A., 2004. Probabilistic tomography maps chemical heterogeneities throughout the mantle. Science 306, 853–856.
Tschauner, O., Huang, S., Greenberg, E., Prakapenka, V.B., Ma, C., Rossman, G.R., Shen, A.H., Zhang, D., Newville, M., Lanzirotti, A., Tait, K., 2018. Ice-VII inclusions in diamonds: evidence for aqueous fluid in Earth's deep mantle. Science 359, 1136–1139.
Valencia-Cardona, J.J., Shukla, G., Wu, Z., Houser, C., Yuen, D.A., Wentzcovitch, R.M., 2017. Influence of the iron spin crossover in ferropericlase on the lower mantle geotherm. Geophys. Res. Lett. 44, 4863–4871.
van Keken, P.E., Hauri, E.H., Ballentine, C.J., 2002. Mantle mixing: the generation, preservation, and destruction of chemical heterogeneity. Annu. Rev. Earth Planet. Sci. 30, 493Ð–525.
Vanderbilt, D., 1990. Soft self-consistent pseudopotentials in a generalized eigenvalue formalism. Phys. Rev. B 41 (11), 7892–7895.
Vočadlo, L., Alfè, D., Gillan, M., Price, G., 2003. The properties of iron under core conditions from first principles calculations. Phys. Earth Planet. Int. 140, 101–125.
Wang, X., Tsuchiya, T., Hase, A., 2015. Computational support for a pyrolitic lower mantle containing ferric iron. Nat. Geosci. 8, 556–560.
Wentzcovitch, R., Karki, B., Cococcioni, M., de Gironcoli, S., 2004. Thermoelastic properties of $MgSiO_3$-perovskite: insights on the nature of the Earth's lower mantle. Phys. Rev. Lett. 92, 018501.
Wentzcovitch, R.M., Justo, J., Wu, Z., da Silva, C., Yuen, D., Kohlstedt, D., 2009. Anomalous compressibility of ferropericlase throughout the iron spin crossover. Proc. Natl. Acad. Sc. USA 106, 8447–8452.
Wentzcovitch, R.M., Yu, Y.G.G., Wu, Z.Q., 2010. Thermodynamic properties and phase relations in mantle minerals investigated by first principles quasiharmonic theory. Theoretical and Computational Methods in Mineral Physics: Geophysical Applications 71, 59–98.
Wicks, J.K., Duffy, T.S., 2016. Crystal structures of minerals in the lower mantle. In: Terasaki, H., Fischer, R. (Eds.), Deep Earth: Physics and Chemistry of the Lower Mantle and Core. Wiley, pp. 69–87.
Williams, Q., 1998. The temperature contrast across D″. In: Gurnis, M., Wysession, E.K., Buffett, B. (Eds.), M. American Geophysical Union, The Core-mantle Boundary Region, pp. 73–81.
Williams, Q., Knittle, E., 2005. The uncertain major element bulk composition of Earth's mantle. In: Earth's Deep Mantle: Structure, Composition, and Evolution. Geophysical Monograph Series 160 AGU.
Wolf, A. S., Jackson, J. M., Dera, P., Prakapenka, V. B., 2015. The thermal equation of state of (Mg,Fe)SiO_3 bridgmanite (perovskite) and implications for lower mantle structures. J. Geophys. Res. 120, 7460–7489.
Wu, Z., 2016. Velocity structure and composition of the lower mantle with spin crossover in ferropericlase. J. Geophys. Res. 121, 2304–2314.
Wu, Z., Wentzcovitch, R., 2014. Spin crossover in ferropericlase and velocity heterogeneities in the lower mantle. Proc. Nat. Academy Sci. 111, 10468–10472.
Wu, Z., Wentzcovitch, R.M., 2017. Composition versus temperature induced velocity heterogeneities in a pyrolitic lower mantle. Earth Planet. Sci. Lett. 457, 359–365.
Wu, Z., Justo, J., da Silva, C., de Gironcoli, S., Wentzcovitch, R.M., 2009. Anomalous thermodynamic properties in ferropericlase throughout its spin crossover transition. Phys. Rev. B 80, 014409.
Wu, Z., Justo, J., Wentzcovitch, R., 2013. Elastic anomalies in a spin-crossover system: ferropericlase at lower mantle conditions. Phys. Rev. Lett. 110, 228501.
Wu, W., Ni, S., Irving, J.C.E., 2019. Inferring Earth's discontinuous chemical layering from the 660-kilometer boundary topography. Science 363, 736–740.
Xu, W., Lithgow-Bertelloni, C., Stixrude, L., Ritsema, J., 2008. The effect of bulk composition and temperature on mantle seismic structure. Earth Planet. Sci. Lett. 275, 70–79.
Yamazaki, D., Karato, S.-I., 2001. Some mineral physics constraints on the rheology and geothermal structure of Earth's lower mantle. Am. Mineral. 86, 385–391.
Yang, R., Wu, Z., 2014. Elastic properties of stishovite and the CaCl2-type silica at the mantle temperature and pressure: an ab initio investigation. Earth Planet. Sci. Lett. 404, 14–21.
Zhong, S., 2006. Constraints on thermochemical convection of the mantle from plume heat flux, plume excess temperature, and upper mantle temperature. J. Geophys. Res. 111, B04409.